NASA Technical Memorandum 4090

The 13-Inch Magnetic Suspension and Balance System Wind Tunnel

William G. Johnson, Jr., and David A. Dress

JANUARY 1989

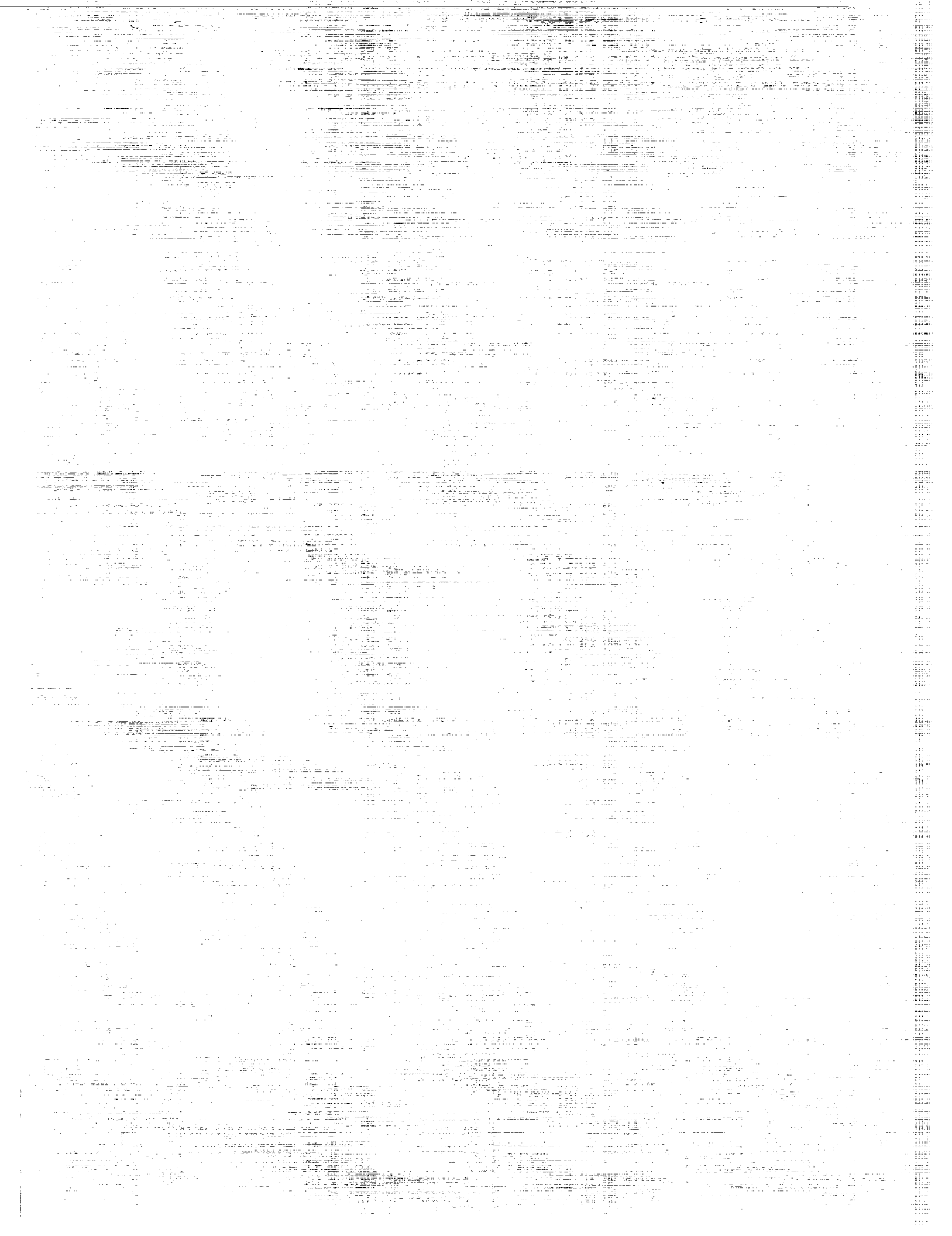

NASA Technical Memorandum 4090

The 13-Inch Magnetic Suspension and Balance System Wind Tunnel

William G. Johnson, Jr., and David A. Dress
Langley Research Center
Hampton, Virginia

National Aeronautics
and Space Administration

**Scientific and Technical
Information Division**

1989

Summary

The Langley Research Center has a small, subsonic wind tunnel in use with the 13-inch Magnetic Suspension and Balance System (MSBS). Design and construction considerations resulted in a modified octagonal test section. The transparent test section allows flow visualization over model spans of 6 to 8 inches and lengths of 8 to 12 inches. The tunnel is capable of speeds up to Mach 0.5 and has predictable and acceptable longitudinal Mach number distributions. Flow uniformity measurements show dynamic pressure variations less than ± 0.25 percent across about 80 percent of the test section area. Measurements of flow angularity in pitch show about 0.5° upflow. Velocity fluctuations in the longitudinal direction are about 0.2 ± 0.1 percent.

Introduction

Model support interference can be a major problem during wind-tunnel testing. References 1 and 2 contain over 175 citations from as early as 1923 which only partially document the severity of this problem. From the mid-1950's to around 1970, researchers regarded Magnetic Suspension and Balance Systems (MSBS) as a solution to the support interference problem. Reference 3 documents many research programs and related facilities developed to make maximum use of the then current MSBS capabilities.

Although some small wind tunnels equipped with MSBS's achieved successful operation, interest in similarly equipped large wind tunnels waned in the early 1970's; this was due primarily to perceived formidable technical and financial barriers. However, recent advancements in related areas of technology have removed some of these barriers. One advancement centers on large superconducting electromagnets needed to support the model and also counteract aerodynamic loads. Another focuses on the superconducting solenoid as a model core (ref. 4) which gives the model the highest possible magnetic moment. Furthermore, feasibility and conceptual design studies (refs. 5, 6, and 7) have produced some innovative MSBS designs. These innovations should significantly reduce the costs of MSBS's for large wind tunnels.

Since the late 1970's, Langley researchers have steadily increased their in-house experience in the design, development, and use of MSBS technology. In 1979, the U.S. Air Force loaned the MSBS located at the Arnold Engineering Development Center (AEDC) (ref. 8) to Langley. The initial use of the system provided operational experience with a working MSBS. It also provided a test bed for position-sensing system development and controls studies. To provide detailed study of the MSBS used with a wind tunnel, the AEDC MSBS was combined with a small low-speed wind tunnel. In 1984, this combination became the 13-inch Magnetic Suspension and Balance System wind tunnel at the Langley Research Center. Ownership of this MSBS has since been transferred to NASA from the Air Force.

This report discusses the physical characteristics, some design considerations, and construction of this tunnel. It also includes data from flow uniformity, flow angularity, and velocity fluctuation measurements.

Symbols

A	cross-sectional area of test section, in^2
b	test section width, in.
M	Mach number
p_{atm}	atmospheric pressure, psi
p_t	total pressure, psi
q	local dynamic pressure for each probe on survey rake (computed with wall static pressure and total pressure from survey rake), psf
q_{av}	average of local dynamic pressures, psf
Δq	incremental dynamic pressure for each probe on survey rake, $q - q_{\text{av}}$, psf
R	radial coordinate of tunnel sections, in.
rms	root mean square
u'	fluctuating velocity component in the streamwise direction, fps
U	mean velocity in the streamwise direction, fps
X	longitudinal coordinate of tunnel sections, in.
y	spanwise distance, in.

Physical Characteristics of Wind Tunnel

The schematic drawing in figure 1 shows the tunnel as a closed-throat, open-circuit design. Ambient air enters from and exhausts to the outdoors. Figure 2 shows where the bellmouth inlet and tunnel exhaust penetrate the building wall. A shed roof, shown in figure 3, protects the tunnel inlet from the

weather. Standard household screening protects the tunnel circuit from outside contaminants.

As stated earlier, the purpose of this tunnel was to provide for detailed study of the MSBS in use with a wind tunnel. Therefore, we assembled the circuit from parts of an existing model wind tunnel and a few sections specifically designed for this use. At the time of the original effort, flow quality considerations were not a primary concern. However, this did change and some of the tunnel sections were later modified to improve flow quality. These changes are included in the description of the individual sections. The discussion that follows describes the tunnel circuit sections as they exist without the background information on their original design approach.

Bellmouth

The bellmouth design uses the coordinates of the ASME long-radius nozzle (ref. 9). This nozzle attaches to a straight duct about 2 1/2 inside diameters long (figs. 4 and 5). The bellmouth has an inside throat diameter of 25 in. and its walls are 3/8-in-thick fiberglass-reinforced epoxy. We made total-pressure surveys prior to this installation in the horizontal and vertical planes at the end of this configuration. From these surveys we computed the very flat, uniform dynamic pressure profiles shown in figure 6. Additional constant diameter ducting extends the circuit to the turn.

Turning Vanes

Both turns are of the design and construction shown in figure 7. The photograph in figure 8 shows that the 25-in-diameter turns contain 16 vanes made of rolled aluminum. The vane installation uses a spacing which varied according to the arithmetic progression in figure 9. Dimmock (ref. 10) developed this method of spacing to provide uniform flow distribution downstream of turns in a gas turbine research apparatus. Other tunnels also successfully use this method of spacing for the turning vanes. They include the RAE 5-Meter Low-Speed Tunnel, the Langley 0.3-Meter Transonic Cryogenic Tunnel, and the National Transonic Facility (NTF) at the Langley Research Center.

Quick Diffuser

A quick diffuser provides the necessary flow expansion into the settling chamber. Figure 10 contains the tabulated coordinates for the quick diffuser contour. The change in diameter from 25 to 35.65 in. produces a diffusion ratio of 2.03. Most quick diffusers require a pressure drop device at the exit of the diffuser to prevent flow separation. Prior work indicated that a 2 1/2-in-thick section of 3/8-in. cell honeycomb would give the necessary pressure drop. However, refinements to the circuit, as discussed in the section "Flow Uniformity," resulted in a combination of honeycomb and three different screens. The first is a 5-in-wide annulus of 40-mesh screen; the second, a 10-in-wide annulus of 50-mesh screen; and the third, a full 20-mesh screen. Figure 10 shows the diffuser contour, current screen arrangement, and honeycomb position.

Settling Chamber

A settling chamber with three 20-mesh screens conditions the flow ahead of the contraction and test section. Flanged Rohm & Haas Plexiglas rings form the sections of the settling chamber. Individual frames with diameters greater than the adjoining Plexiglas flange support the screens. Bolts which pass through the Plexiglas flanges and screens join the sections together. This design allows random installation or removal of screens without changing the total length of the section. The sketch in figure 11 shows the original dimensions and screen locations. Different screen locations, also shown in figure 11, were necessary as a result of a later change in the contraction design.

Contraction

The contraction portion of the tunnel consists of two separate contraction sections. The first section (primary) is the more conventional configuration which provides a circle to circle contraction. Figure 12 shows the first section of both the original and modified contractions. The discussion on flow uniformity gives reasons for the modification. Both designs have a contraction ratio of 4.30. The second section (extended), built specifically for this tunnel, completes the transition from a 17.2-in. diameter to the modified octagonal test section. Figure 13 is a schematic drawing of this extended contraction. This design resulted in a contraction ratio of 1.96. The design uses straight-line elements between the section ends. The same geometry serves both as the extended contraction and first-stage diffuser downstream from the test section. The total contraction ratio of the combined contraction sections is 8.43.

Test Section

The first requirement in the design of this tunnel was a decision on test section size and shape. This section needed to be compatible with the existing magnetic suspension and balance system and other existing circuit components. We made the first test section of Plexiglas for ease in viewing the model and in using different types of flow visualization. A later change to General Electric Lexan increased the impact resistance.

Figure 14 shows one of the first shapes considered, a typical square with corner fillets. Because the test section had to fit through the existing circular drag coil, this shape limited the test section area. Its corners and associated joints also created potential interference problems for the X-ray position-sensing system being used at that time. This X-ray system had the source and sensor elements mounted in a $\times$-configuration at 35° from the vertical.

Another early configuration was a regular decagon, also shown in figure 14. This configuration resulted in the largest test section area and placed a flat surface nearly parallel to the position-sensing elements. However, the joint along the side did not offer the clearest viewing area for flow visualization and photographic requirements.

The final configuration removed the side joint from the regular decagon resulting in the modified octagon shown in figure 14. This change caused only a 10-percent decrease in the cross-sectional area. It also provided a good match with the position-sensing elements and a good side view for visual and photographic purposes. Figure 15 shows a schematic drawing of the test section. The major and minor axes for this modified octagon are 12.56 and 10.69 in., respectively. The photograph in figure 16 shows the test section as it passes through the magnet array.

Diffuser

The first-stage diffuser consists of a transition section with the same geometry as the extended contraction discussed earlier. The diffuser half-angle for the top and bottom walls is 2.60° and 3.65° for the sidewalls. This section connects to the main diffuser shown in figure 17. The diffuser half-angle for this section is 2.12°.

Drive fan

The circuit has a 2 1/2-in-thick honeycomb at the end of the main diffuser to protect the fan. A turn similar to the upstream turn directs the flow to the fan section and tunnel exit.

The fan shown in figure 18 has 14 compressor-style blades (3 3/4 in. long) and 15 stators. A water-cooled, 200-hp, 6000-rpm, variable-frequency electric motor drives the fan. The Able Corporation, Anaheim, California, designed and built this very specialized high-power-density motor. Its design and small case diameter of 7.5 in. allowed installation in line with the fan. Figure 19 is a sketch of this installation.

Construction Materials

The circuit components are small, easily handled sections of fiberglass-reinforced epoxy, wood, or Plexiglas. Wooden carts with casters support each section for ease of movement during assembly and maintenance. The carts have leveling screws for positioning and stability once assembled.

Computations From Streamtube Curvature Program

Before we constructed the new tunnel sections, which included the extended contraction, we ran the General Electric Streamtube Curvature Program of reference 11 to predict the longitudinal and cross-sectional Mach number distributions. These computations used that portion of the tunnel circuit from the settling chamber to the end of the first diffuser section. We modeled the area progression of the tunnel as axisymmetric, equivalent area circles. The code used a design value of 0.5 for the test section Mach number. Figure 20 shows the predicted flow as well behaved through the extended contraction. The results also show the expected moderate Mach number increase through the nondiverging test section. The agreement shown between centerline and wall distributions suggests uniform Mach number across the tunnel sections. Two obvious exceptions exist. The first exception occurs in the region of high wall curvature in the primary contraction section. The second exception occurs at the breaks in the wall angle at the start and end of the test section. With no indication of problems resulting from use of the extended contraction design, we assembled the tunnel circuit shown in figure 21.

Calibration of Wind Tunnel

After assembly, we completed some circuit integrity runs. We applied yarn tufts to the tunnel walls from the quick diffuser to the end of the test section. These tufts provided a rough assessment of the flow and indicated reasonably good flow in the test section. However, we saw some flow separation on the settling chamber wall just upstream of the contraction.

During these runs, we used a camera pod installation at the beginning of the contraction as shown in figure 22. This blockage caused minor changes to the area progression between the design and operational stages. Therefore, the Streamtube Curvature Program was rerun with the initial boundary-layer thickness estimated as 1 inch. We installed static-pressure orifices along the same tunnel sections included in the code. We recorded pressures through a range of rpm settings up to the one resulting in a test section Mach number of 0.5. Figure 23 presents the predicted and experimentally determined longitudinal Mach number distributions. The agreement is good except in the diffuser region. This area of

disagreement comes from differences between the actual diffuser sidewall angle and the larger effective diffuser angle as determined from equivalent areas in the code.

Flow Uniformity

We used a cruciform-shaped total-pressure rake to survey the test section for flow uniformity at several longitudinal stations. These results, shown in figure 24, are for intervals of 500 rpm from 500 to 4500 rpm at stations near the beginning and end of the test section. The data show good flow uniformity for almost all rpm settings. The exceptions are the high rpm settings which correspond to the very highest Mach numbers. The data are very similar through the length of the test section. The only differences are the result of expected boundary-layer growth.

The original intent of our research was to gain some practical experience with a MSBS. Therefore, we considered the flow characteristics defined from this initial survey as satisfactory. However, after some basic testing, we determined that improved flow quality would be necessary to obtain useful aerodynamic data. When the original calibration data were reexamined as q distributions (see fig. 25 for $M \approx 0.49$ data), we noted undesirable variations up to ± 1.6 percent in q across the test section. The general distribution was quite unsymmetrical with the maximum deviation near the top wall.

As a start to improving the flow quality, we established a goal of ± 0.25-percent variation in the q distribution. The survey station shown in figure 15 was the location of all the measurements used for evaluating improvements in flow uniformity. We suspected that some of the large deviations in figure 25 were a result of the camera pod and strut installation. The first step was to remove the camera pod and strut. Before doing a new survey, we installed a 0.25-in-diameter pitot tube at the previous location of the strut. This replaced the reference total-pressure tube originally installed in the upstream end of the camera pod. The results in figure 26 show considerable improvement in the q distribution for the middle area of the test section.

For additional improvement, we added three 20-mesh screens at the end of the quick diffuser to increase the pressure drop (fig. 27). The results from this change appear in figure 28. The maximum deviation is about 1.1 percent near the top wall and the horizontal survey is now symmetrical.

After studying the data and the tunnel setup, we realized that the wake from the pitot probe was influencing the bottom results. We pulled this tube down next to the tunnel wall and did another survey. (Note that the measurement of a reference total pressure is not necessary for determining variation in q in the test section.) Figure 29 shows the vertical and horizontal distributions as symmetrical. The maximum deviation is about 0.8 percent. The wake from the pitot tube appears to have increased the total-pressure loss measured near the bottom of the test section. Interestingly, the absence of the deficit after lowering the probe provides strong evidence of no swirl in the flow.

We tried modifying the screen and honeycomb combination at the end of the quick diffuser. Different modifications gave varying degrees of success. Figure 30 shows the screen and honeycomb arrangement that resulted in the least variation in q. The data in figure 31 show that the maximum deviation for this arrangement is 0.5 percent, which is a significant improvement over the previous maximum of 0.8 percent; however, we were aiming for 0.25 percent.

We finally determined that a modification to the primary contraction contour was necessary to meet the desired level of flow uniformity. This contraction was an existing piece originally intended for use as a quick diffuser. By design, it quickly turned and slowed the flow with a small radius of curvature surface. In reverse, this section when used as a contraction section appeared to overaccelerate the flow. This resulted in higher velocity regions near the walls of the test section. This is clear in most of the surveys where the peaks in the q variation represent the highest velocities. Therefore, we decided to increase the radius of curvature by fairing in the entrance of the primary contraction section.

Figures 12(b) and 32 show the lines of the modified primary contraction. We interchanged the two constant diameter sections of the settling chamber to give additional length for a fairing. We then made a smooth transition between the last screen of the settling chamber and the beginning of the extended contraction section.

We surveyed the flow resulting from the modified primary contraction and the screen-honeycomb arrangement in figure 32. Figure 33 shows the results of this survey. The deviations in q are within ± 0.25 percent over about 80 percent of the width and height of the test section. Although more improvements in flow quality may be possible, we made no additional effort to optimize the screen-honeycomb arrangement following the contraction modification.

The last step was the installation of a new total-pressure–total-temperature probe in the contraction at an off-axis location. The 0.125-in-diameter probe reduces down to 0.063 in. in diameter after the 90° turn to minimize its wake.

Flow Angularity

We used the high sensitivity two-axis yawmeter shown in figure 34 to measure flow angularity. The manufacturer's data show the sensitivity for this probe as about an order of magnitude higher than conventional five-tube designs (ref. 12). For this study, we mounted the yawmeter to one of the test section sidewalls as shown in figure 35. This yawmeter gives the flow direction in both pitch and yaw planes as well as the total pressure. We recorded pressures in both pitch and yaw planes at three spanwise stations for Mach numbers up to 0.4.

The reference for the yawmeter's pitch attitude was an optical cathetometer leveled to horizontal zero. This is a remote fixed device used to measure relative vertical and horizontal displacements. (See fig. 36.) With the use of this device, the pitch attitude was accurate to about $\pm 0.02^\circ$. Due to the lack of accurate measurements of the yawmeter's yaw attitude, we did not include the results in the yaw plane.

Figure 37 shows the flow angularity results in the pitch plane at three spanwise stations. It is important to note that these angles are relative to the cathetometer reference and not the test section centerline and indicate an upflow of about 0.5°. Since the tunnel sections rest on stands that are not fixed to the floor, they are free to move. Measurements of the tunnel floor angle made during the flow angularity runs show the tunnel floor angle to vary from 0.05° to 0.15°. Therefore, the flow angularity relative to a tunnel reference could be as low as 0.35°.

Velocity Fluctuations

We used a constant-temperature hot-wire anemometer to measure the fluctuating velocity component in the streamwise direction u'. The commercially available single-wire probe used 0.00015-in-diameter platinum-coated tungsten wire with a sensor length of 0.050 in. We took data through a Mach number range from 0.05 to 0.3 in a plane perpendicular to the test section centerline. This plane was located longitudinally at the magnet center in the test section. Since it is generally accepted that the flow is incompressible for Mach numbers below 0.3, we assumed King's Law to be appropriate for calibration of the wire and for data reduction.

Calibration data at each survey location were fitted by a regression analysis to the King's Law equation:

$$E^2 = A + BV^n$$

where E is the mean voltage, V is the mean velocity, and A, B, and n in this equation are constants determined by the regression analysis. Figure 38 shows a typical data set and curve fit.

In the data reduction, each instantaneous voltage from the hot wire is added to its direct-current component and then converted to an instantaneous velocity. These instantaneous velocities are then collectively analyzed to determine the rms values. The rms values, in percent, are plotted as a function of Reynolds number for the horizontal and vertical centerlines in figure 39. The data show a fluctuation level of 0.2 ± 0.1 percent in the streamwise component.

Concluding Remarks

Sections of an existing model tunnel were combined with some new sections to produce a small, subsonic wind tunnel with very good flow qualities. We used this tunnel in conjunction with the 13-inch Magnetic Suspension and Balance System (MSBS). The tunnel is capable of speeds up to Mach 0.5. We were able to predict the longitudinal Mach number distributions through the test section by using the General Electric Streamtube Curvature Program. Refinements to the circuit resulted in dynamic pressure variations of ± 0.25 percent or less across about 80 percent of the test section area. Measurements of flow angularity in pitch show about 0.5° upflow. Velocity fluctuations in the longitudinal direction are about 0.2 ± 0.1 percent.

NASA Langley Research Center
Hampton, VA 23665-5225
December 9, 1988

References

1. Tuttle, Marie H.; and Gloss, Blair B.: *Support Interference of Wind Tunnel Models—A Selective Annotated Bibliography.* NASA TM-81909, 1981. (Corrected 1988.)
2. Tuttle, Marie H.; and Lawing, Pierce L.: *Support Interference of Wind Tunnel Models—A Selective Annotated Bibliography.* Supplement to NASA TM-81909, 1984. (Corrected 1988.)
3. Tuttle, Marie H.; Kilgore, Robert A.; and Boyden, Richmond P.: *Magnetic Suspension and Balance Systems—A Selected, Annotated Bibliography.* NASA TM-84661, 1983. (Supersedes NASA TM-80225.)
4. Britcher, C.; Goodyer, M. J.; Scurlock, R. G.; and Wu, Y. Y.: A Flying Superconducting Magnet and Cryostat for Magnetic Suspension of Wind Tunnel Models. *Cryogenics*, vol. 24, no. 4, Apr. 1984, pp. 185–189.
5. Bloom, H. L.; et al.: *Design Concepts and Cost Studies for Magnetic Suspension and Balance Systems.* NASA CR-165917, 1982.
6. Boom, R. W.; Eyssa, Y. M.; McIntosh, G. E.; and Abdelsalam, M. K.: *Magnetic Suspension and Balance System Study.* NASA CR-3802, 1984.

7. Boom, R. W.; Eyssa, Y. M.; McIntosh, G. E.; and Abdelsalam, M. K.: *Magnetic Suspension and Balance System Advanced Study.* NASA CR-3937, 1985.
8. Matthews, R. K.; Brown, M. D.; and Langford, J. M.: *Description and Initial Operation of the AEDC Magnetic Model Suspension Facility: Hypersonic Wind Tunnel (E).* AEDC-TR-70-80, U.S. Air Force, May 1970. (Available from DTIC as AD 869 634.)
9. Shoop, Charles F.; and Tuve, George L.: *Mechanical Engineering Practice—A Laboratory Reference Text,* Fifth ed. McGraw-Hill Book Co., Inc., 1956.
10. Dimmock, N. A.: *The Development of a Simply Constructed Cascade Corner for Circular Cross Section Ducts.* National Gas Turbine Establ. Memo. No. 78, British Ministry of Supply, Feb. 1950.
11. Ferguson, D. R.; and Keith, J. S.: *Modifications to the Streamtube Curvature Program. Volume I—Program Modifications and User's Manual.* NASA CR-132705, 1975.
12. Bryer, D. W.; and Pankhurst, R. C.: *Pressure-Probe Methods for Determining Wind Speed and Flow Direction.* Her Majesty's Stationery Off. (London), 1971.

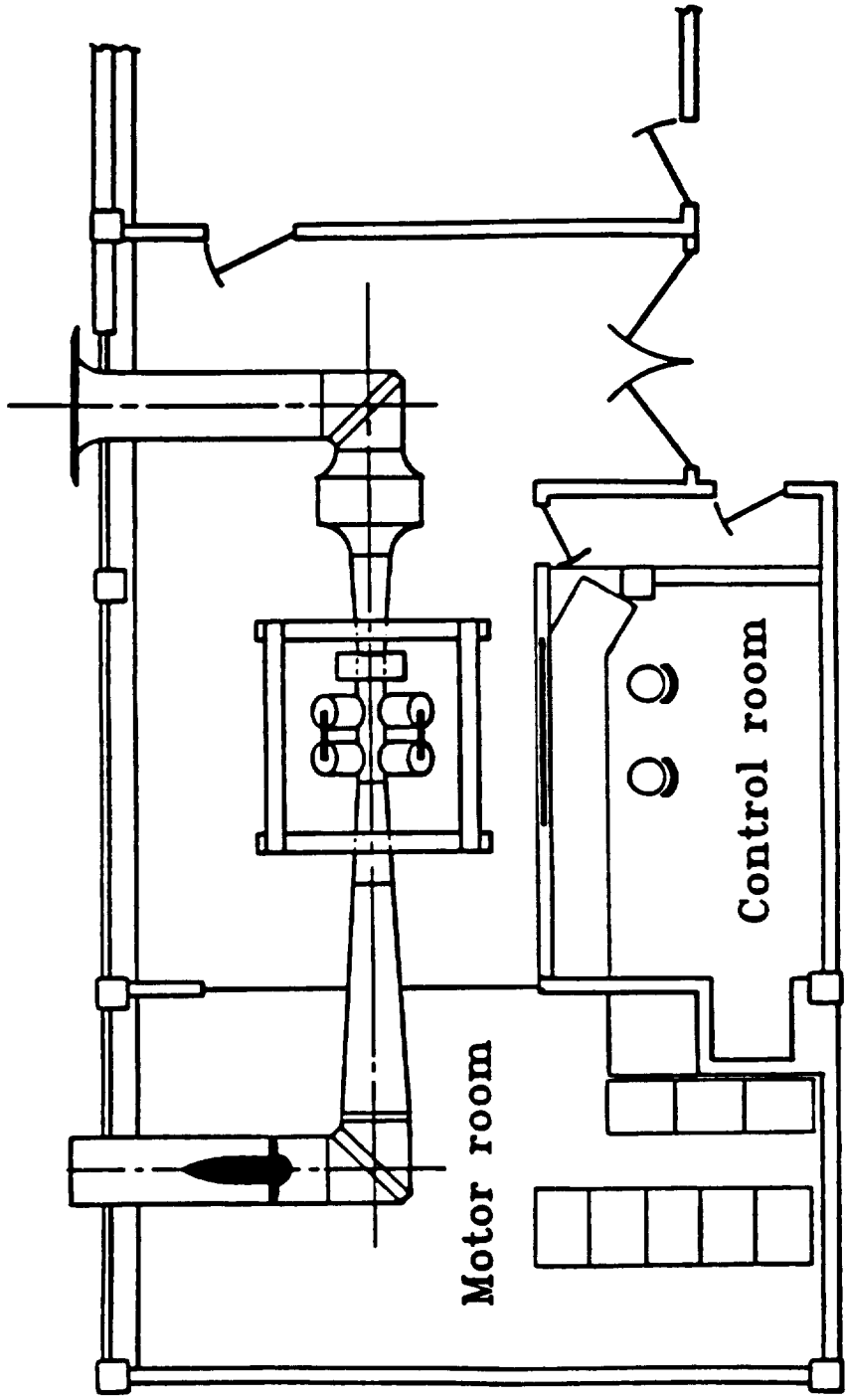

Figure 1. Floor plan showing tunnel circuit and MSBS.

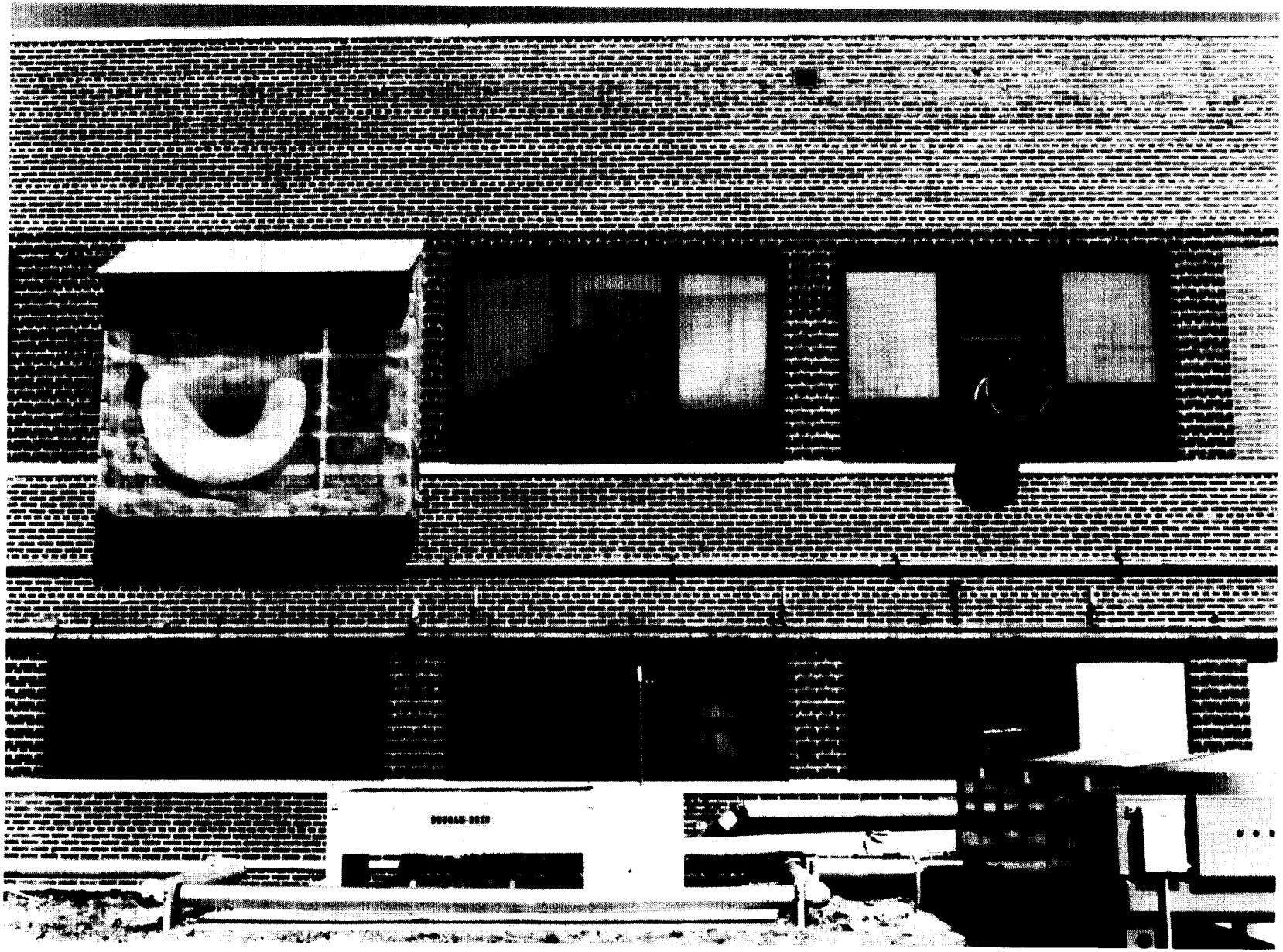

L-87-02379

Figure 2. Building elevation showing tunnel inlet and exhaust.

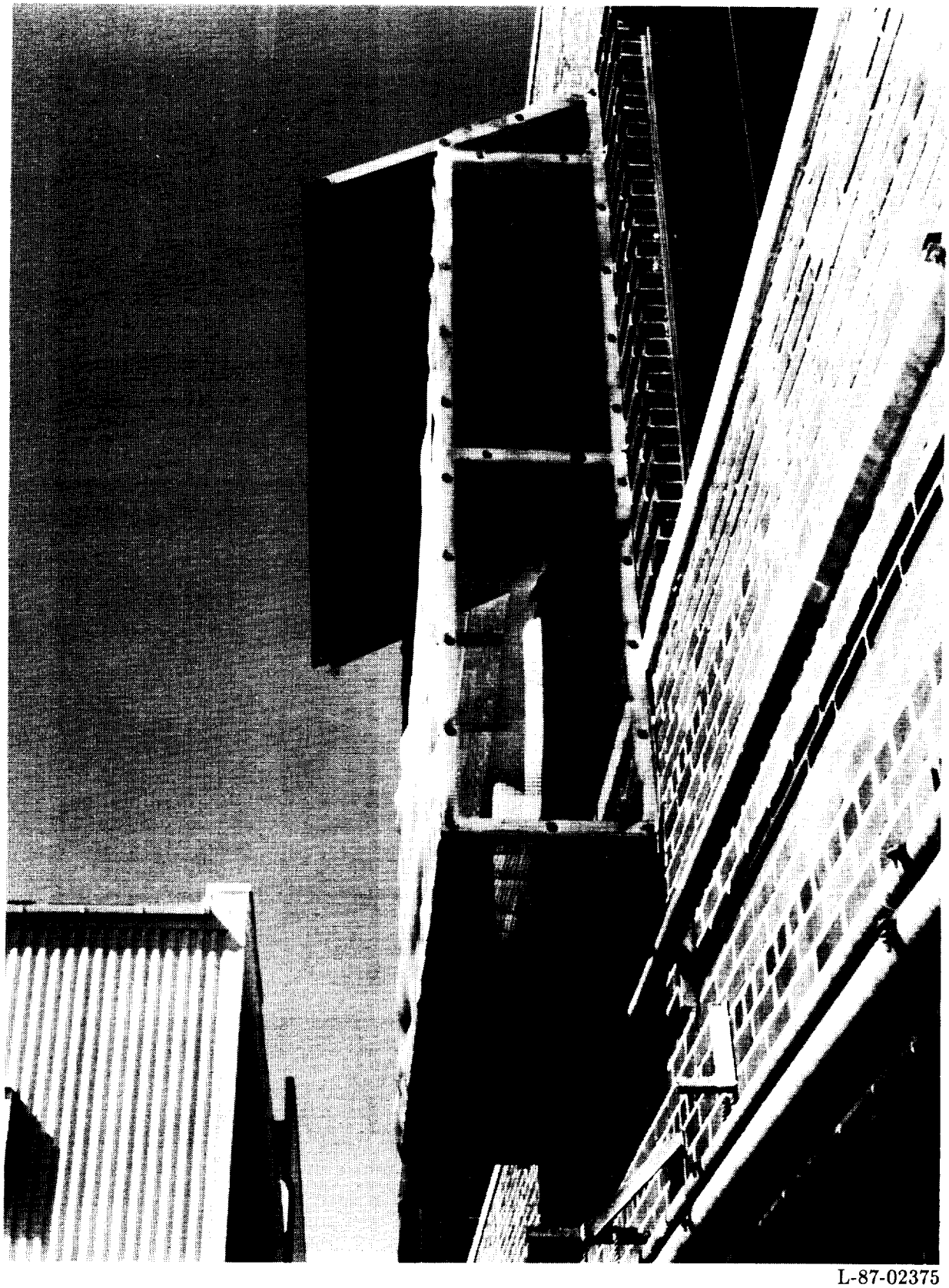

L-87-02375

Figure 3. Tunnel inlet enclosure.

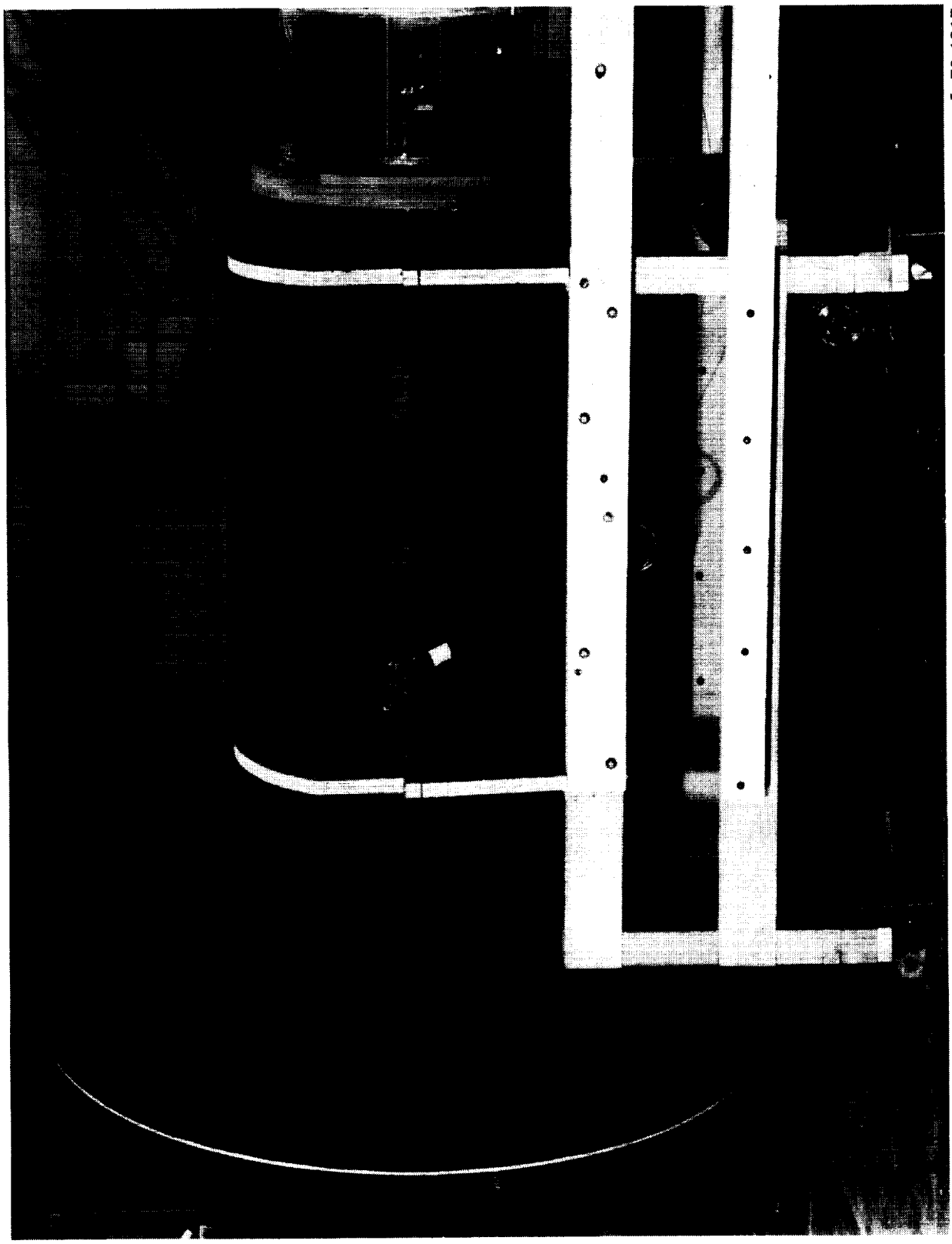

L-76-1217

Figure 4. Bellmouth inlet.

BELLMOUTH COORDINATES			
X, in.	R, in.	X, in.	R, in.
0.00	12.50	19.71	18.91
2.56	12.59	21.46	20.62
5.13	12.86	22.82	22.34
7.68	13.30	23.80	24.03
10.26	13.96	24.45	25.74
12.83	14.92	24.87	27.47
15.38	16.02	25.00	29.18
17.40	17.21		

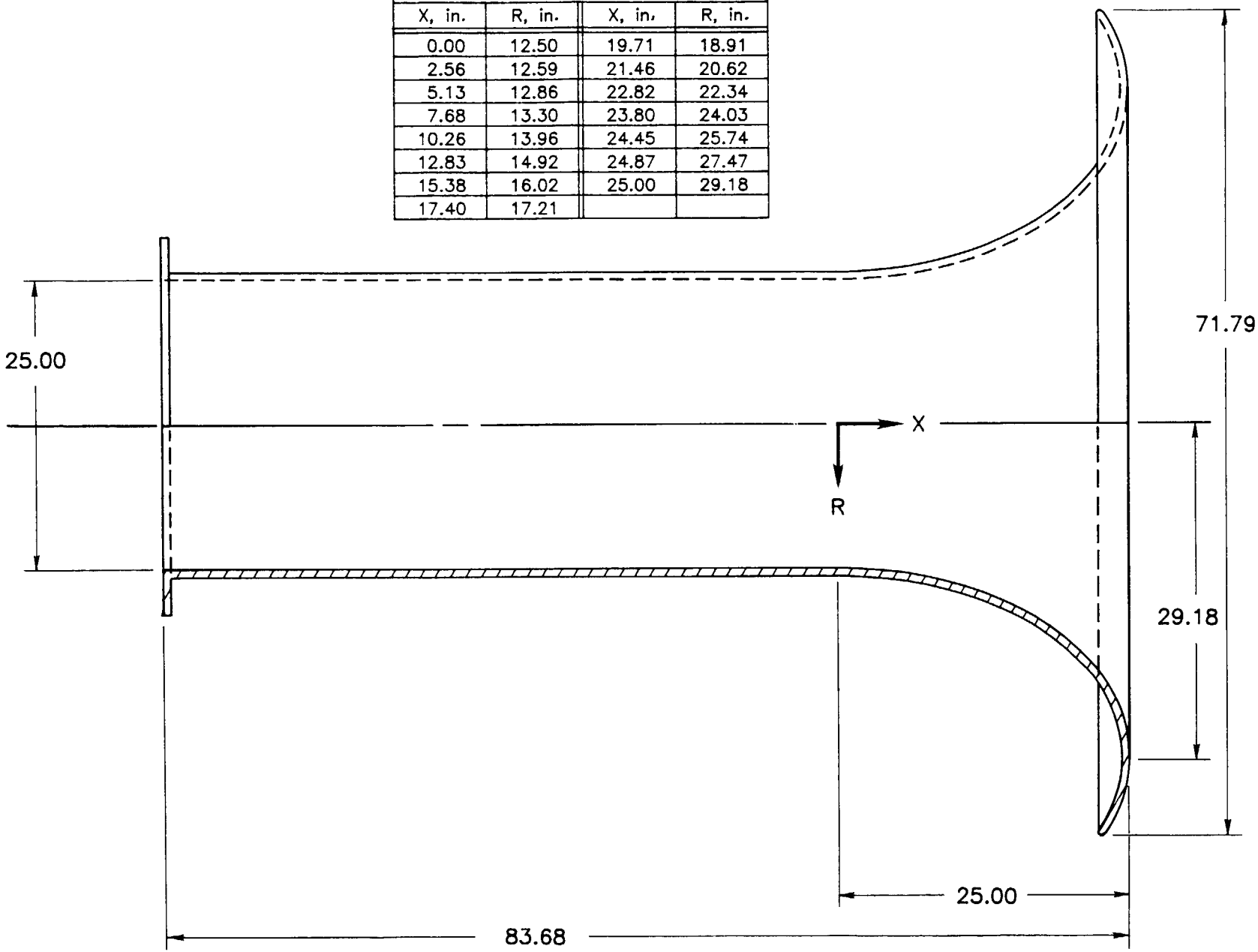

Figure 5. Drawing of MSBS inlet bellmouth. Dimensions are in inches.

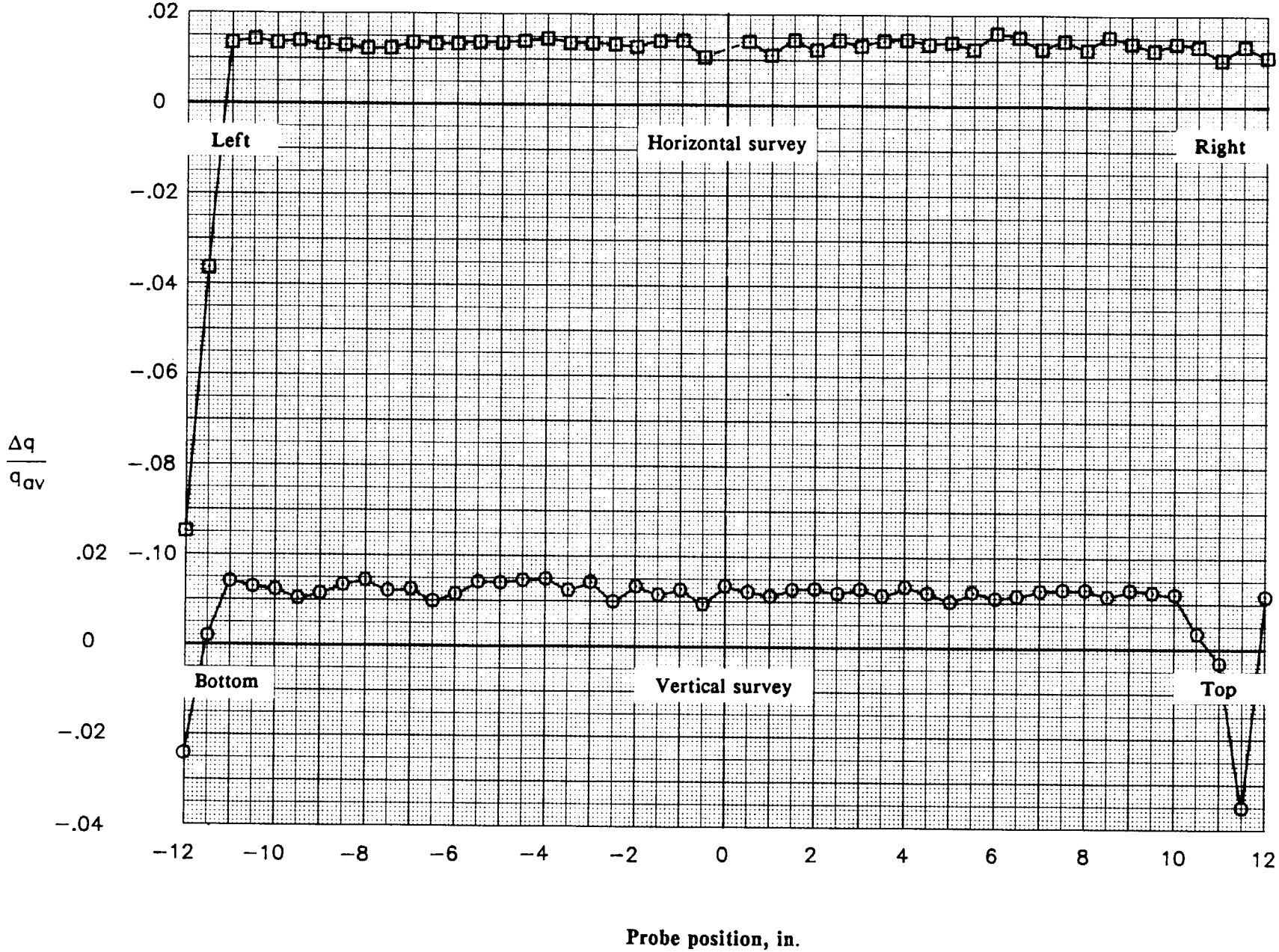

Figure 6. Dynamic pressure profiles at downstream end of bellmouth.

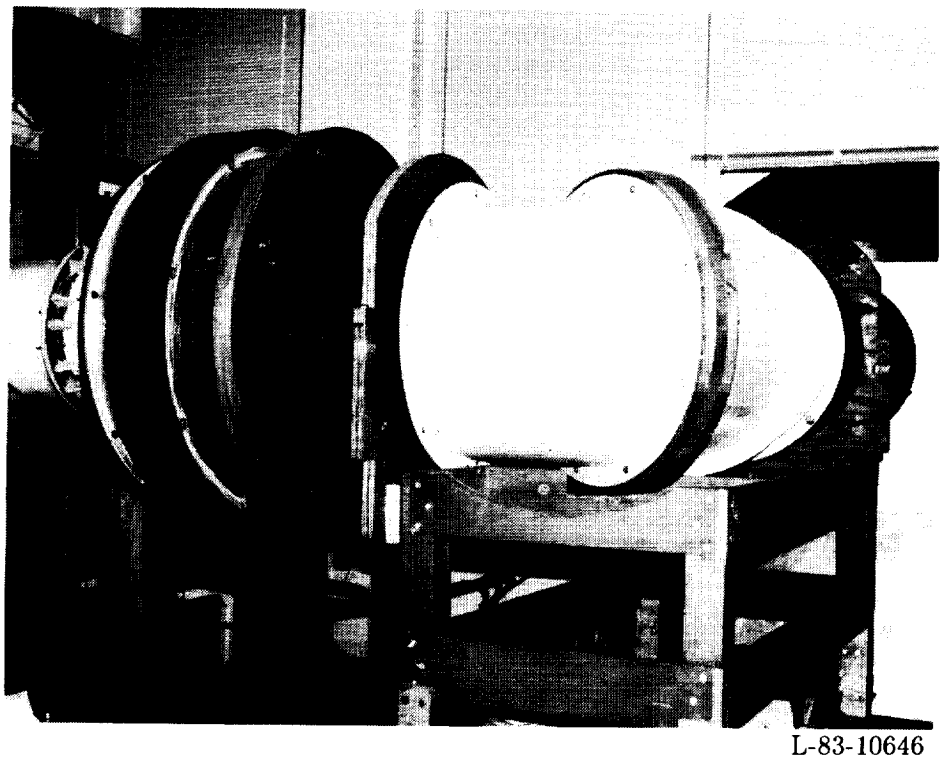

L-83-10646

(a) Upstream turn.

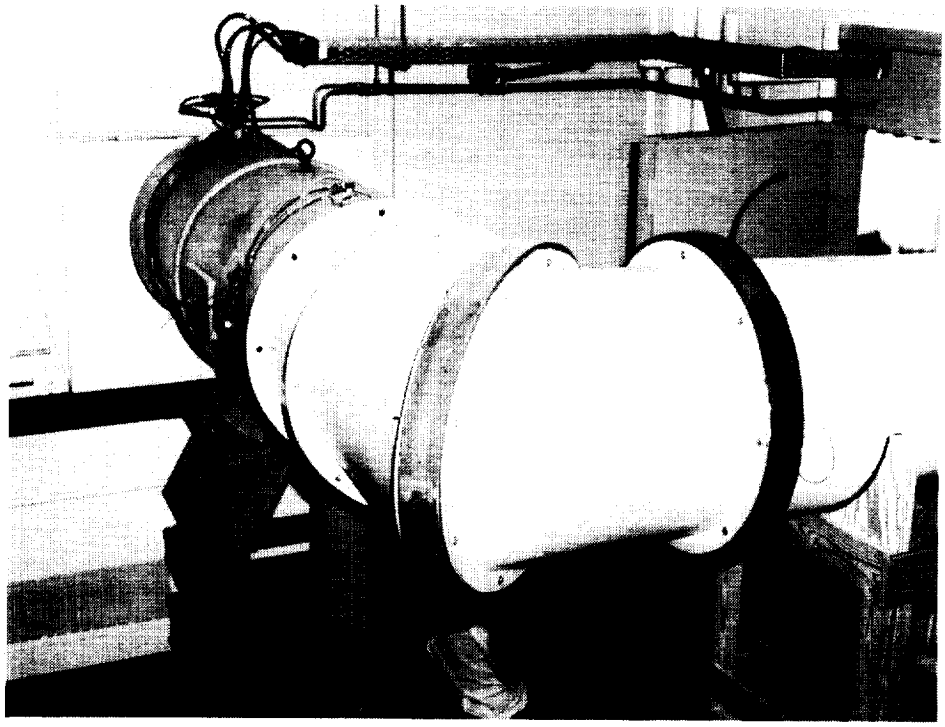

L-83-10647

(b) Downstream turn.

Figure 7. The 13-inch MSBS tunnel turns.

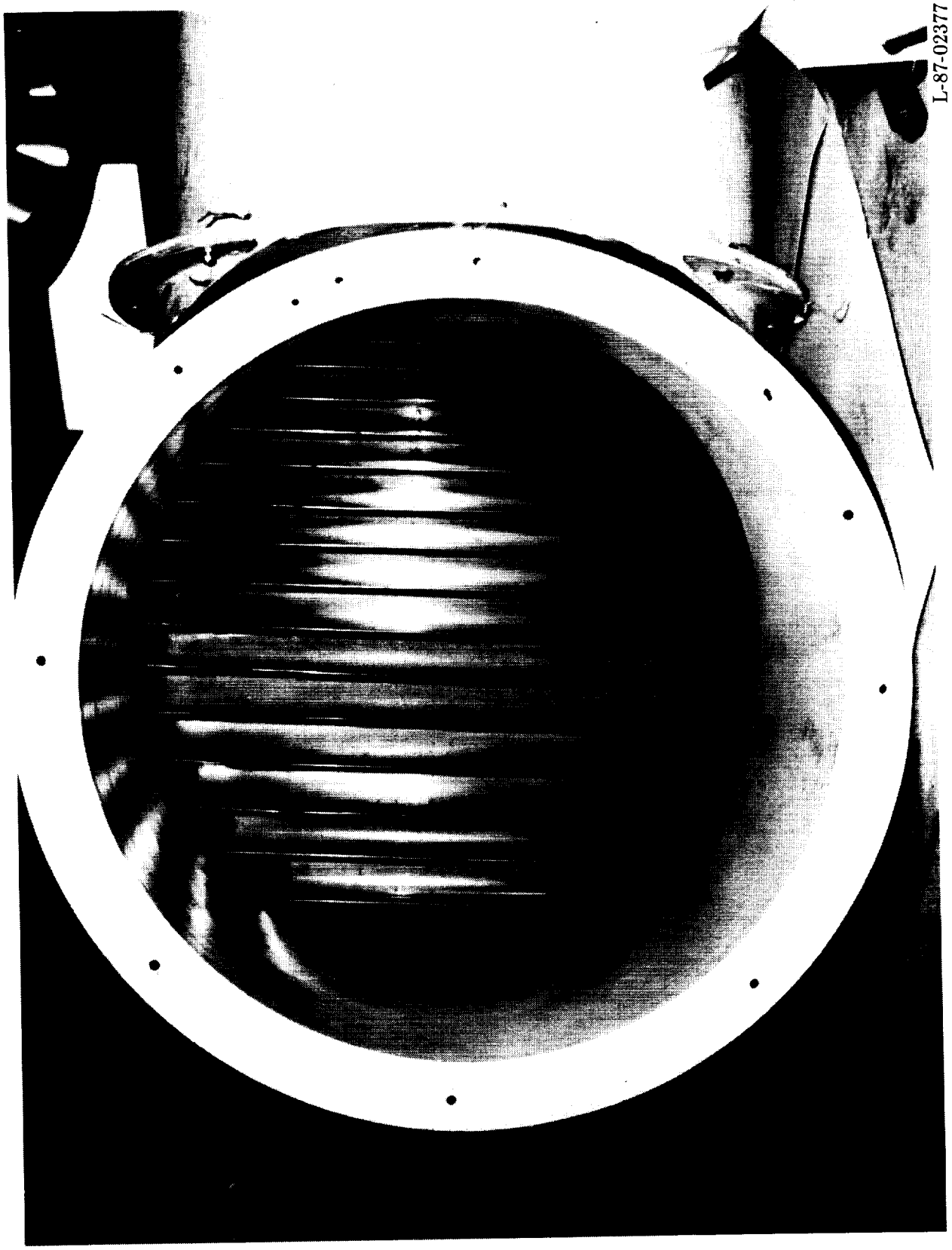

L-87-02377

Figure 8. Upstream face of turning-vane assembly.

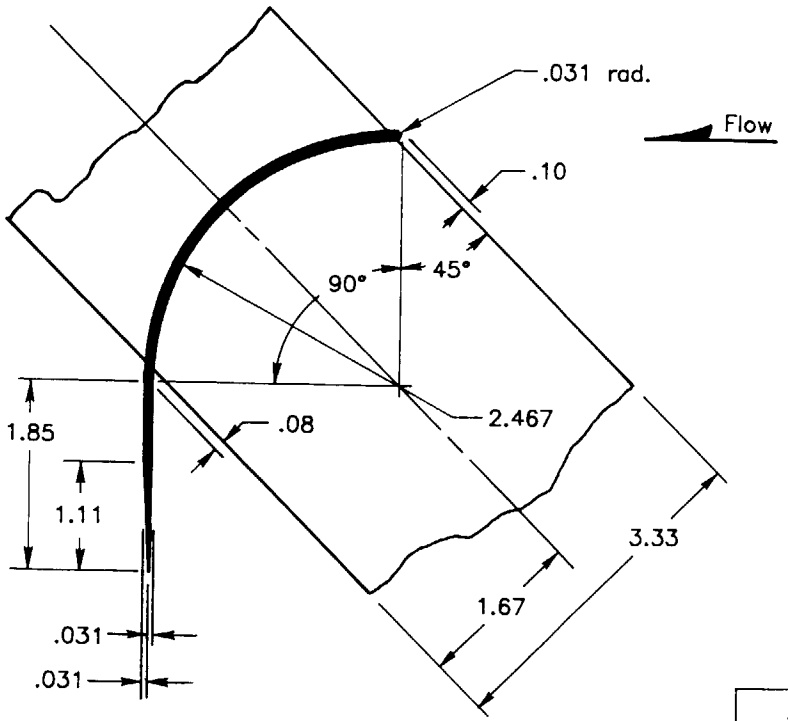

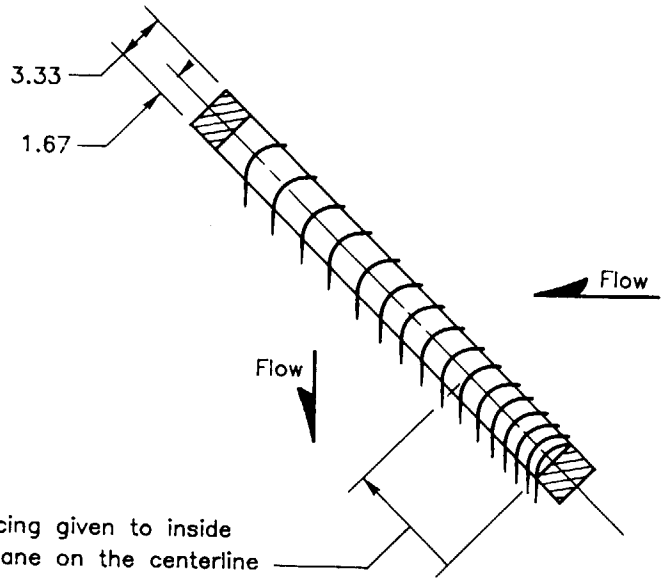

Vane spacing given to inside surface of vane on the centerline

Vane Number	Spacing	Vane Number	Spacing
1	.73	9	13.24
2	1.73	10	15.53
3	2.88	11	17.98
4	4.21	12	20.59
5	5.69	13	23.38
6	7.34	14	26.31
7	9.14	15	29.40
8	11.11	16	32.66

Figure 9. Details of turning-vane assembly. Dimensions are in inches.

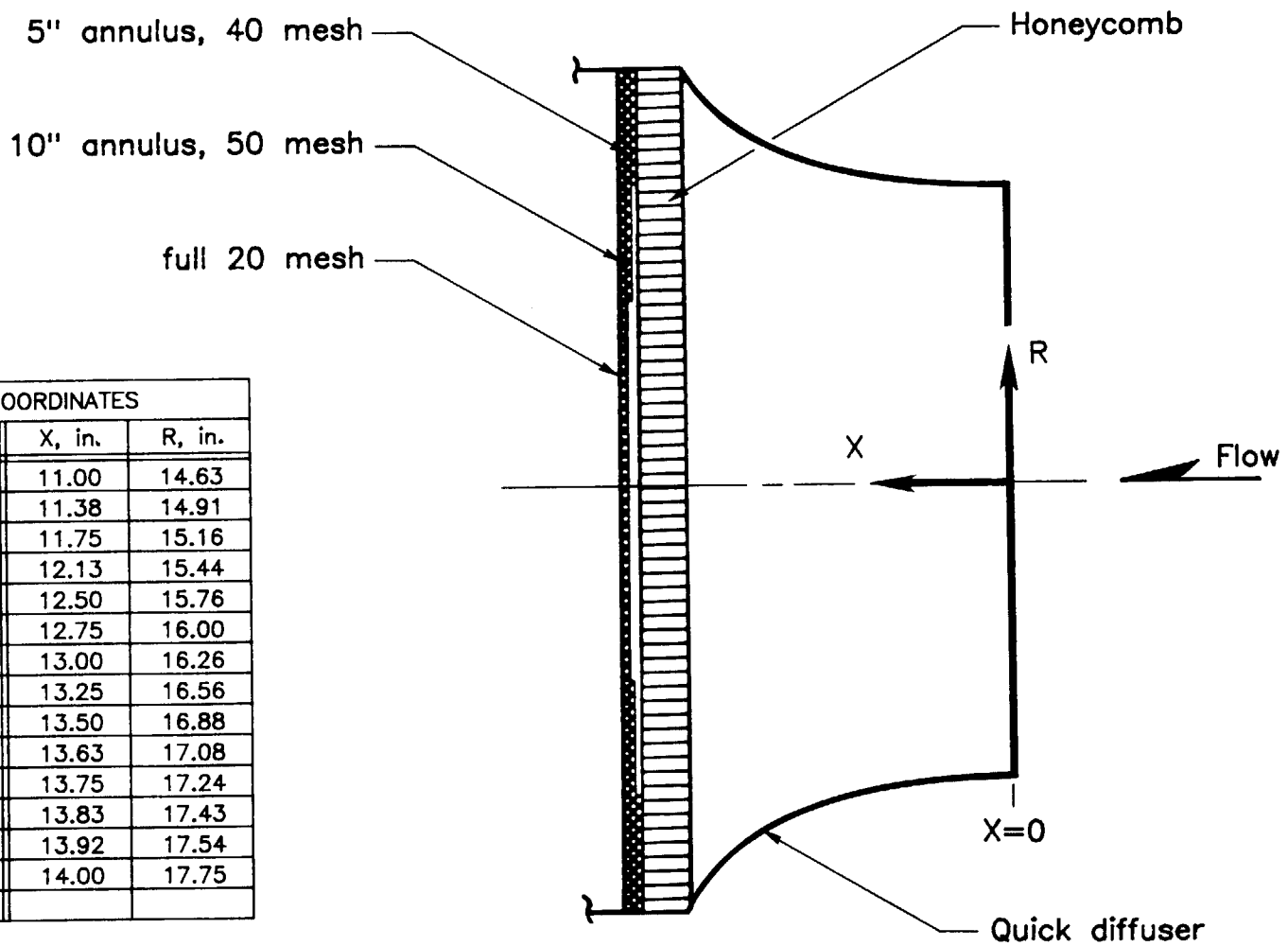

DIFFUSER COORDINATES			
X, in.	R, in.	X, in.	R, in.
0.00	12.50	11.00	14.63
1.00	12.51	11.38	14.91
2.00	12.56	11.75	15.16
3.00	12.63	12.13	15.44
4.00	12.72	12.50	15.76
5.00	12.84	12.75	16.00
5.75	12.95	13.00	16.26
6.50	13.09	13.25	16.56
7.25	13.26	13.50	16.88
8.00	13.45	13.63	17.08
8.50	13.60	13.75	17.24
9.00	13.77	13.83	17.43
9.50	13.96	13.92	17.54
10.00	14.17	14.00	17.75
10.50	14.41		

Figure 10. Quick diffuser configuration and coordinates.

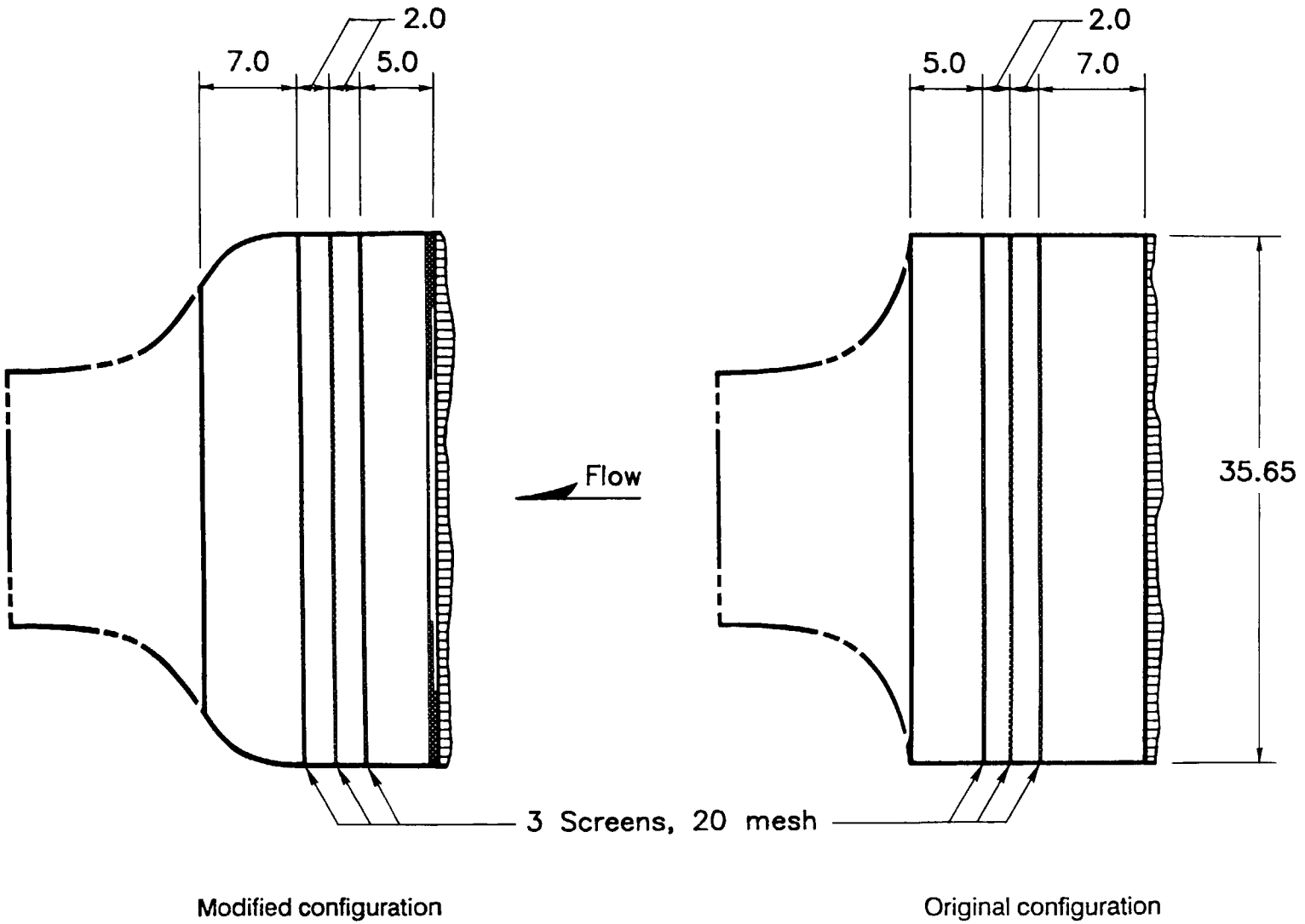

Figure 11. Settling chamber configurations with screen locations. Dimensions are in inches.

CONTRACTION COORDINATES			
X, in.	R, in.	X, in.	R, in.
0.00	17.83	3.28	10.48
0.08	17.53	3.48	10.32
0.28	16.78	3.68	10.17
0.48	16.03	3.88	10.03
0.68	15.29	4.38	9.74
0.88	14.56	4.88	9.50
1.08	13.94	5.38	9.32
1.28	13.41	5.88	9.17
1.48	12.96	6.38	9.05
1.68	12.55	6.88	8.96
1.88	12.19	7.88	8.83
2.08	11.87	8.88	8.74
2.28	11.58	9.88	8.69
2.48	11.31	10.88	8.65
2.68	11.07	11.88	8.62
2.88	10.86	12.88	8.60
3.08	10.66	13.63	8.60

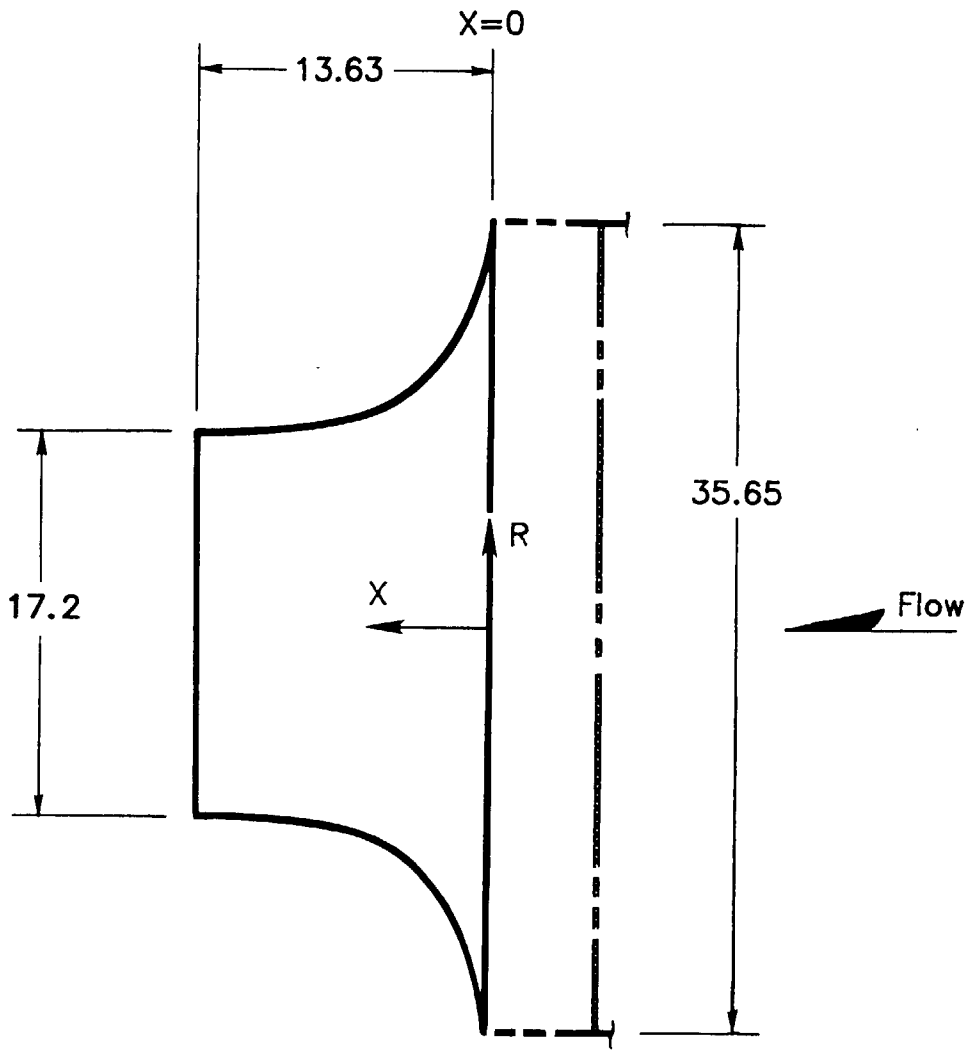

(a) Original configuration.

Figure 12. Primary contraction configurations and coordinates. Dimensions are in inches.

CONTRACTION COORDINATES			
X, in.	R, in.	X, in.	R, in.
−7.00	17.83	4.00	9.97
−6.00	17.83	5.00	9.47
−5.00	17.78	6.00	9.15
−4.00	17.65	7.00	8.95
−3.00	17.35	8.00	8.82
−2.00	16.68	9.00	8.74
−1.00	15.62	10.00	8.69
0.00	14.35	10.88	8.65
1.00	13.01	11.88	8.62
2.00	11.75	12.88	8.60
3.00	10.72	13.63	8.60

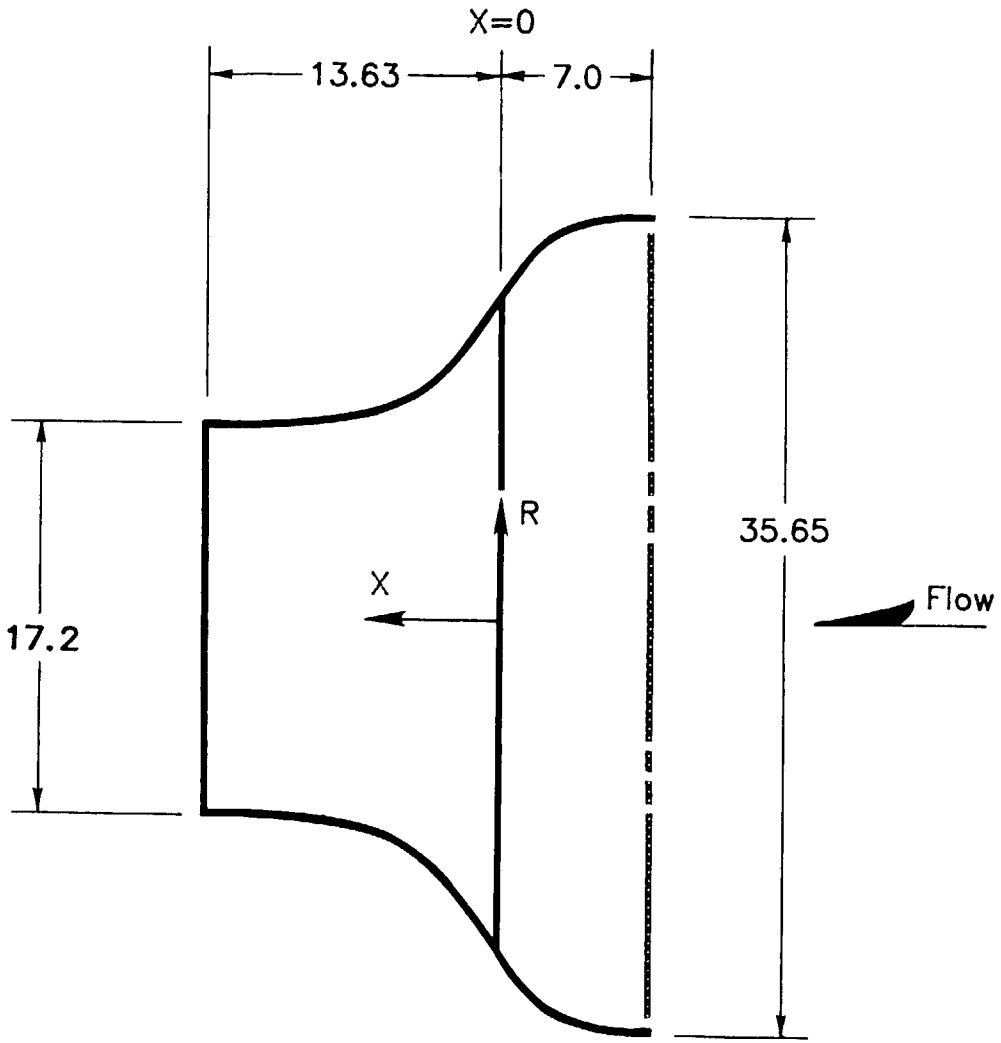

(b) Modified configuration.

Figure 12. Concluded.

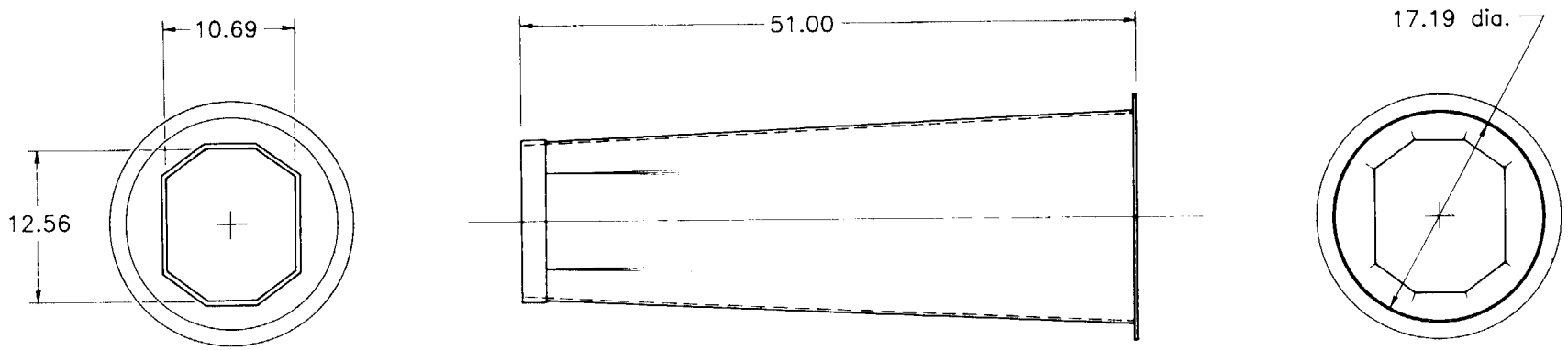

Figure 13. Transition section used as extended contraction and first-stage diffuser. Dimensions are in inches.

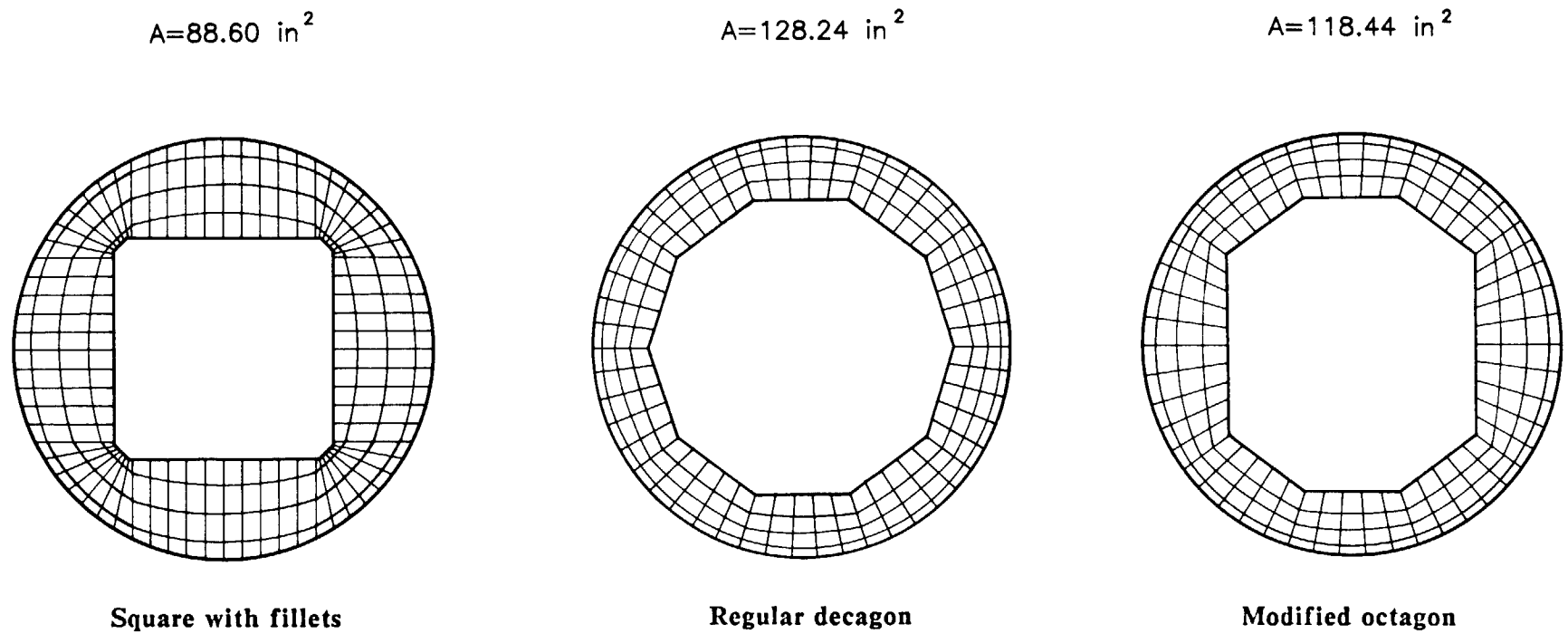

Figure 14. Shapes considered for test section cross section.

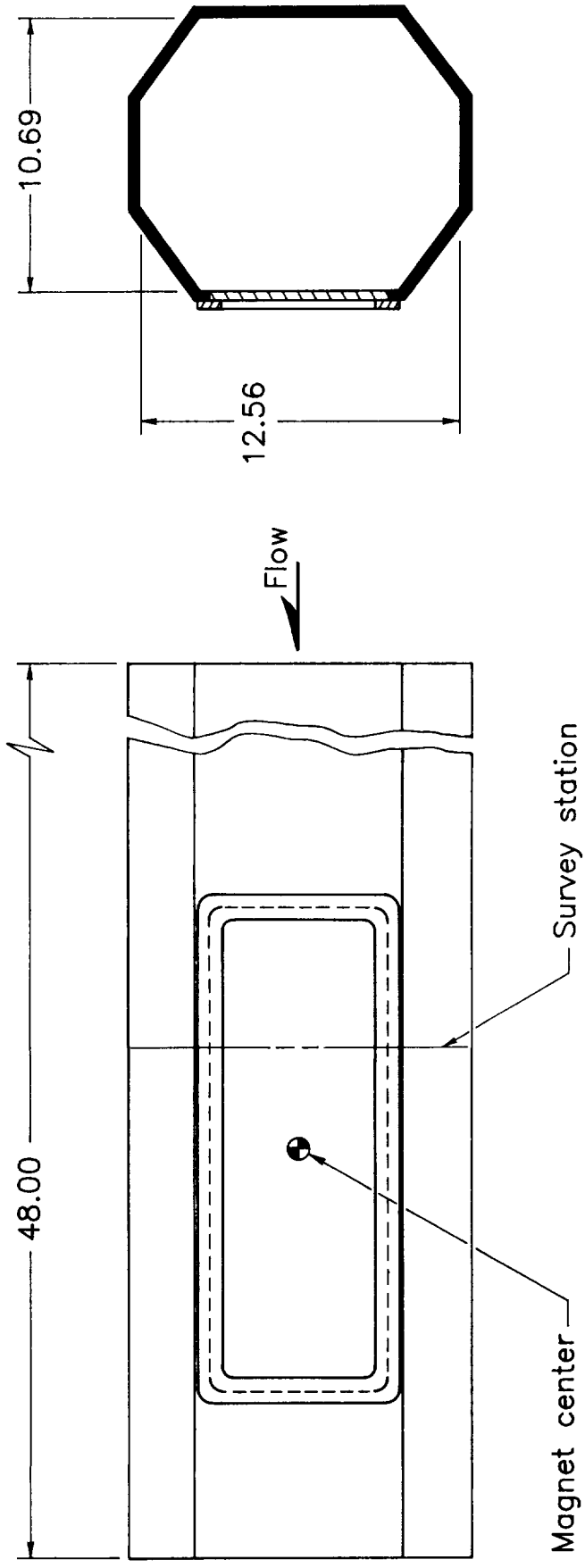

Figure 15. The 13-inch MSBS wind-tunnel test section. Dimensions are in inches.

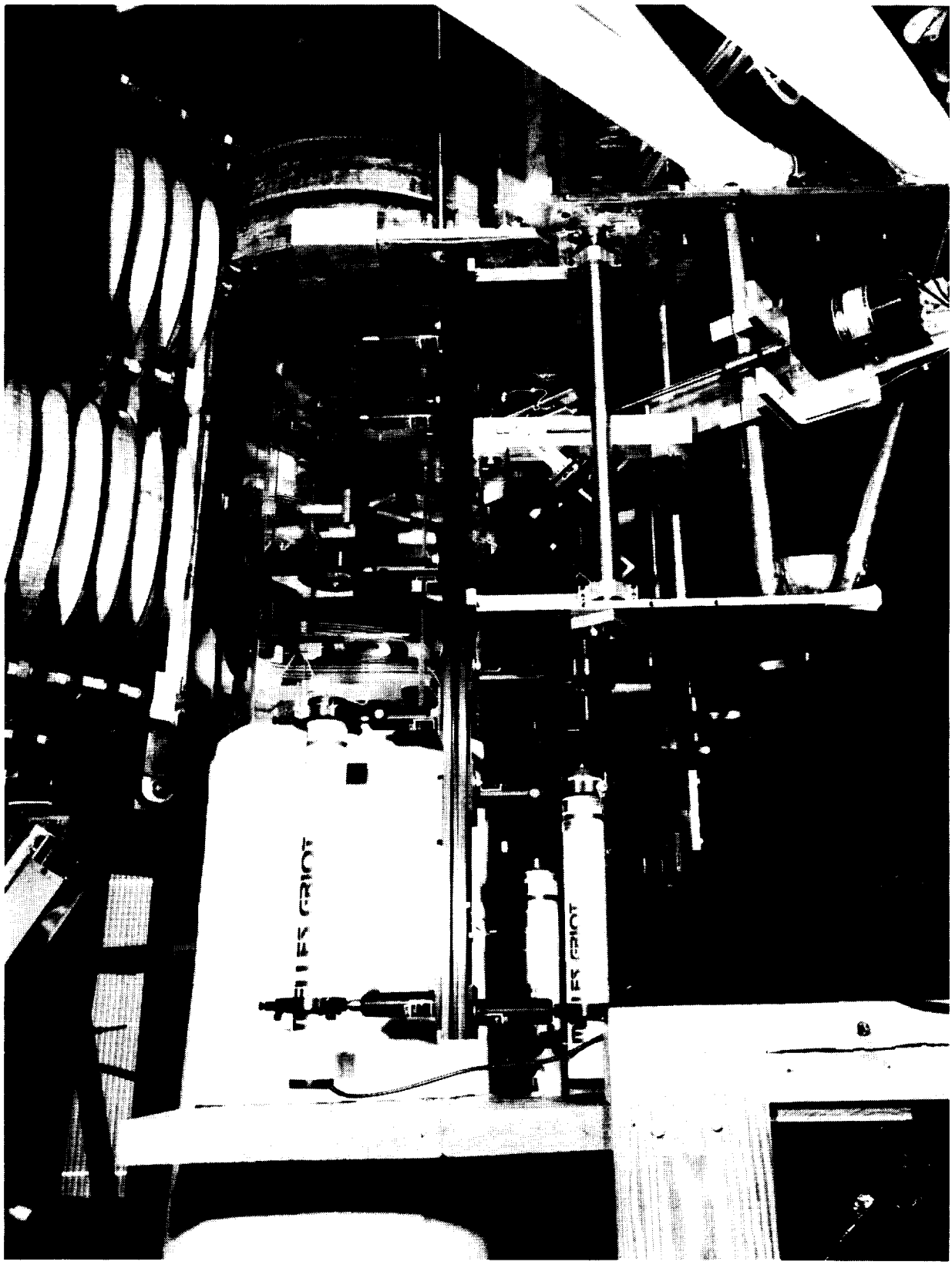

L-84-8806

Figure 16. Test section as installed in magnet array.

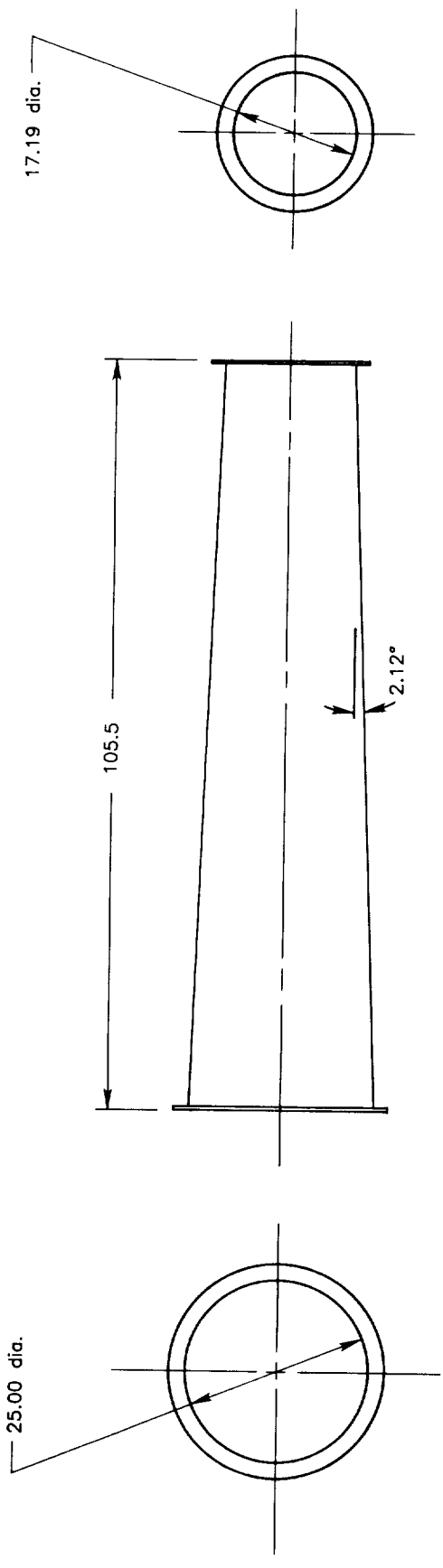

Figure 17. Main diffuser geometry. Linear dimensions are in inches.

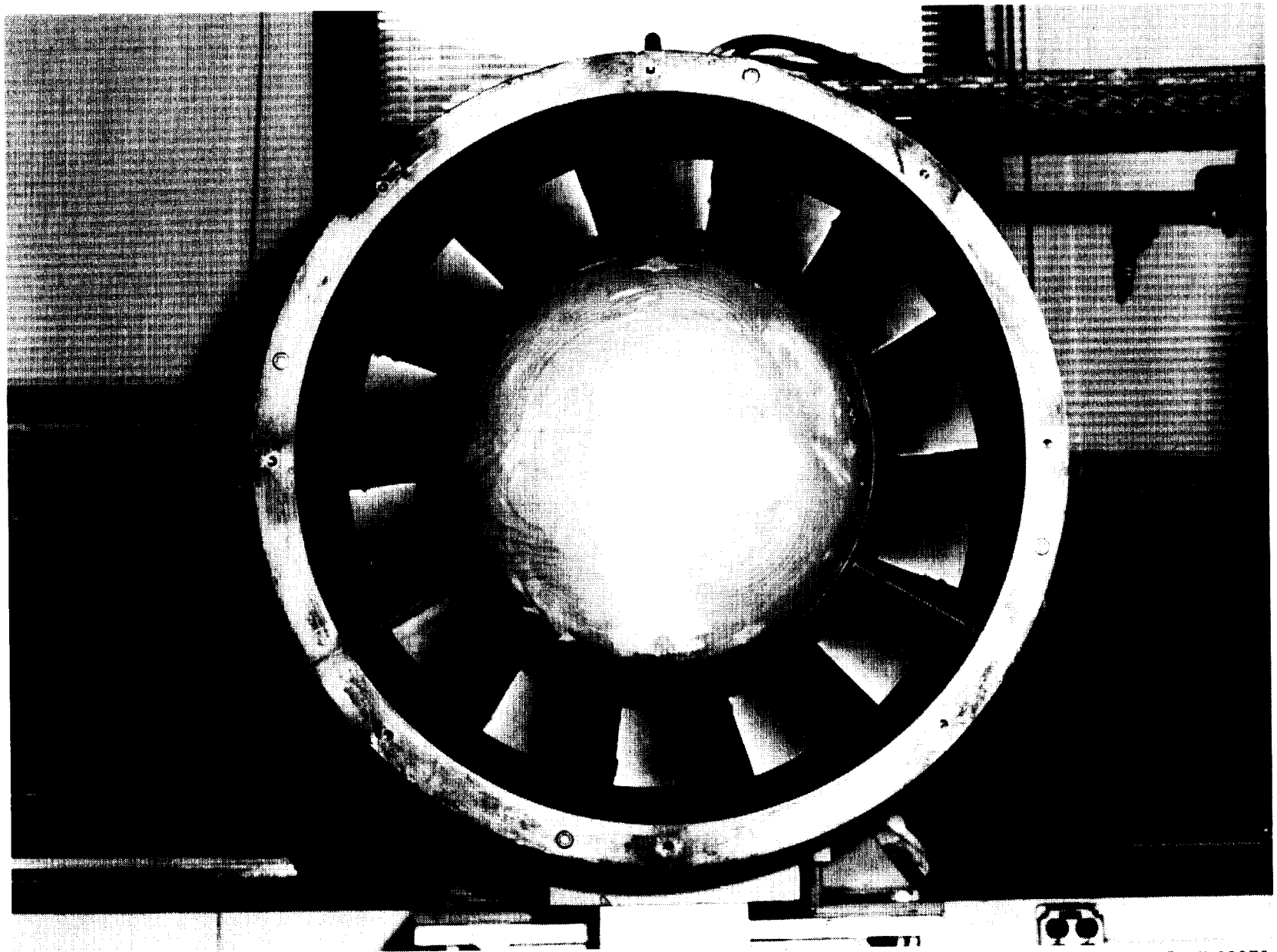

L-87-02376

Figure 18. Upstream face of drive fan.

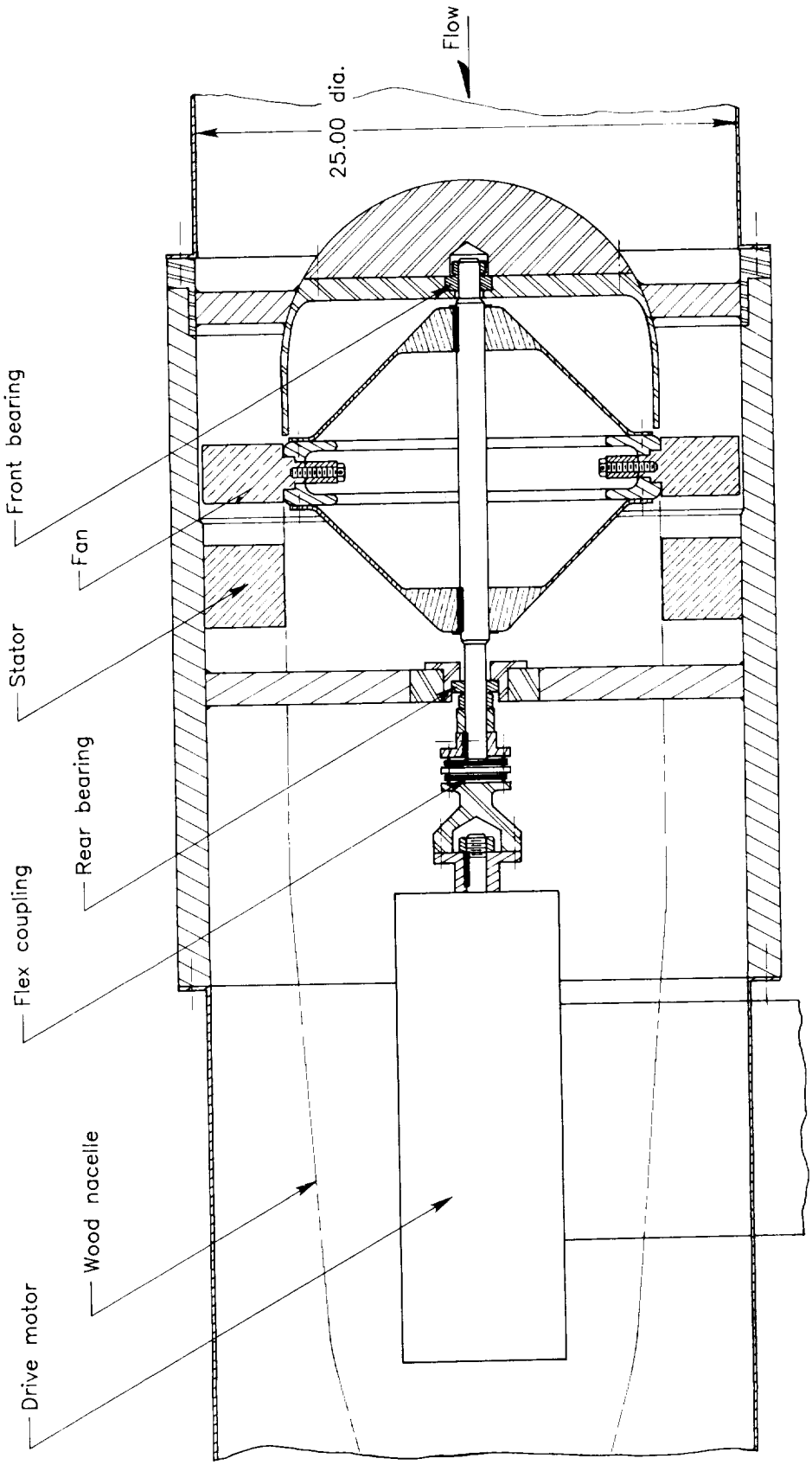

Figure 19. Schematic drawing of drive fan installation. Dimensions are in inches.

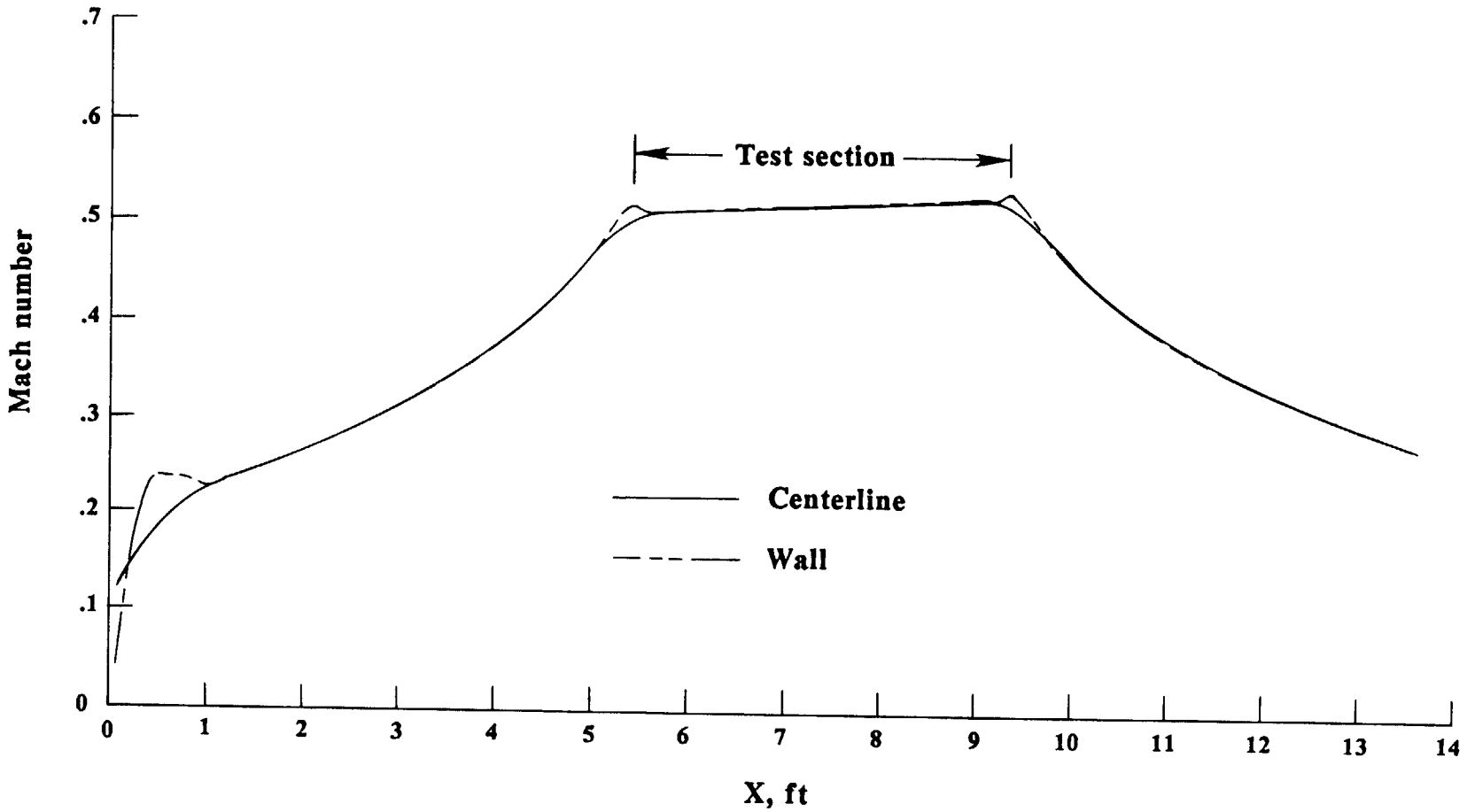

Figure 20. Longitudinal Mach number distribution as predicted by Streamtube Curvature Program.

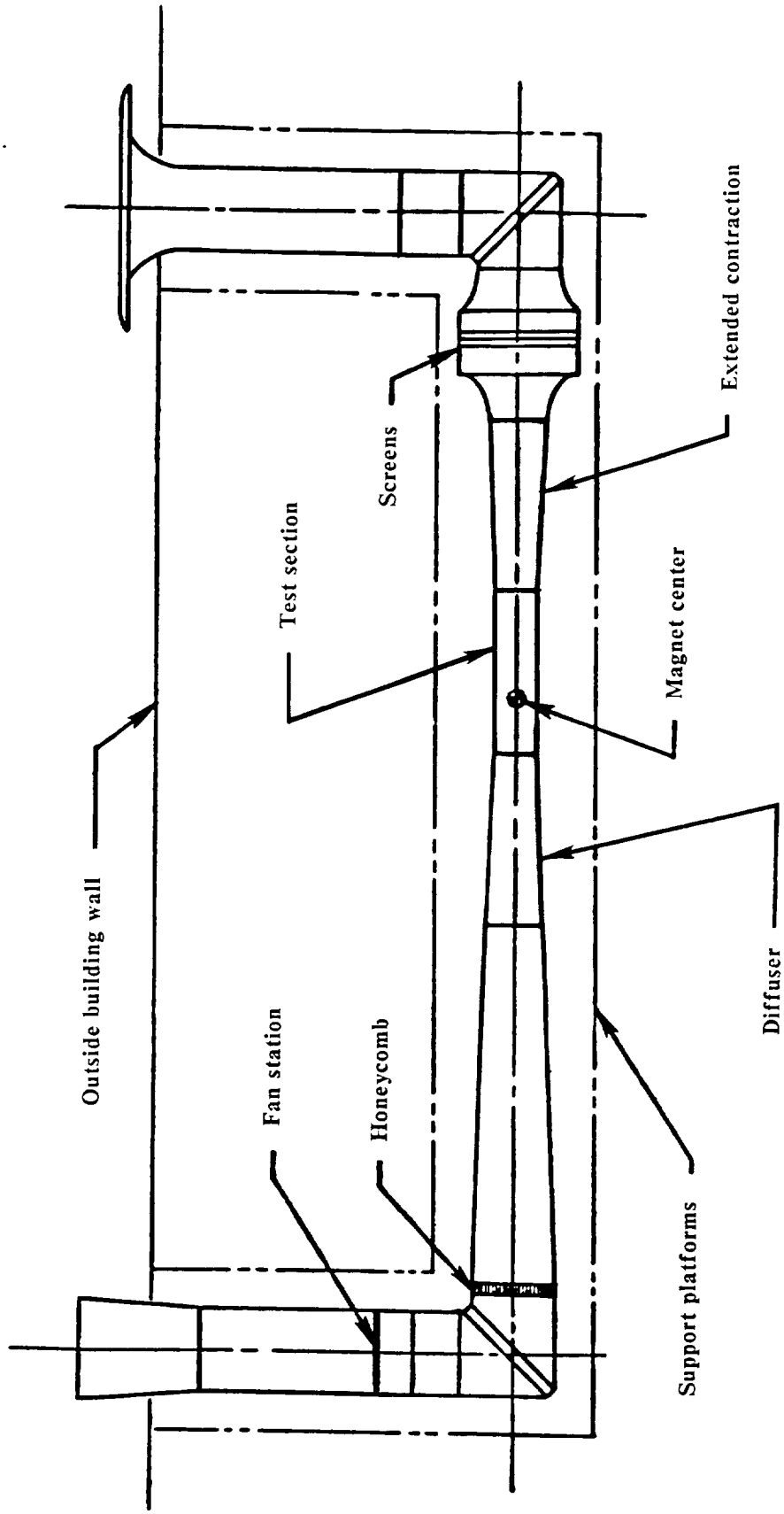

Figure 21. The 13-inch MSBS wind-tunnel layout.

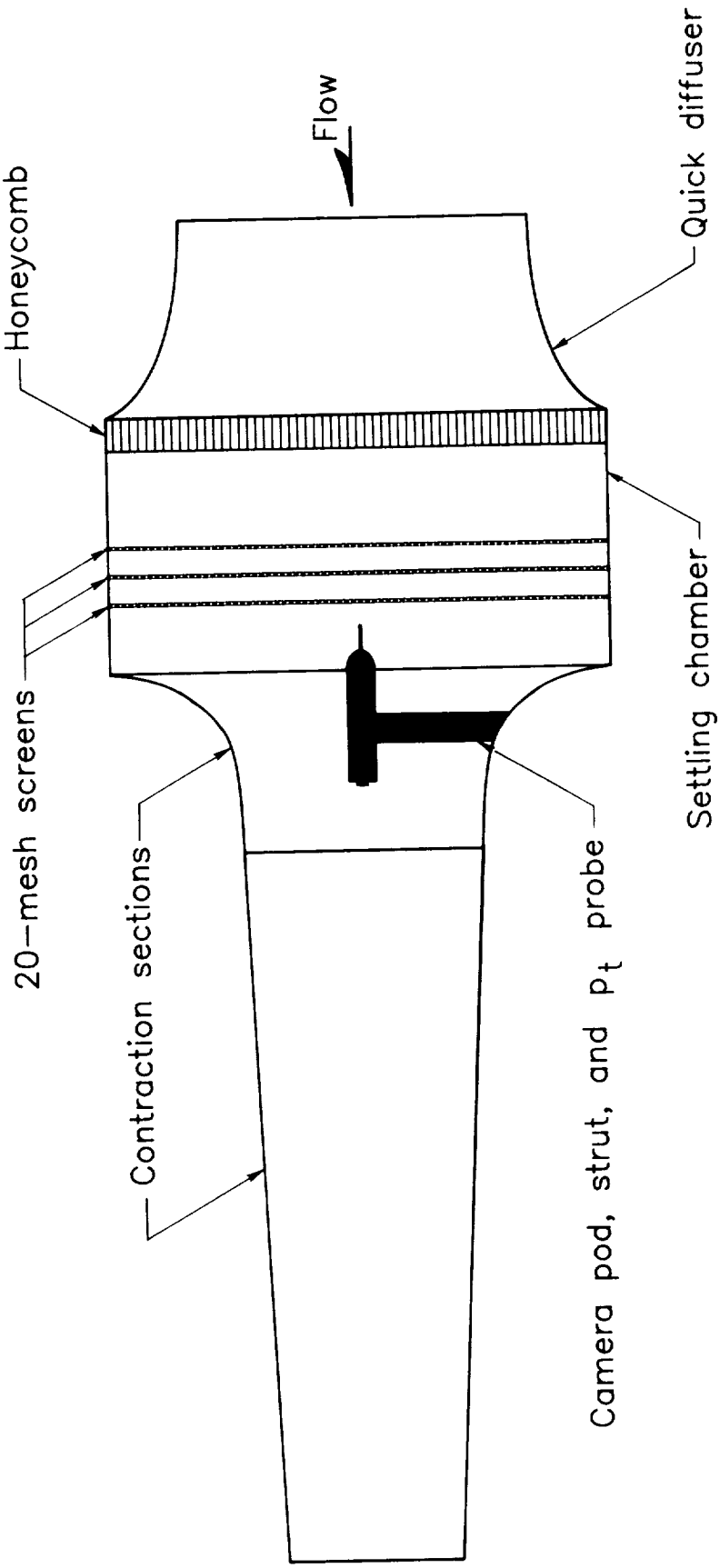

Figure 22. Quick diffuser, settling chamber, and contraction sections before modification.

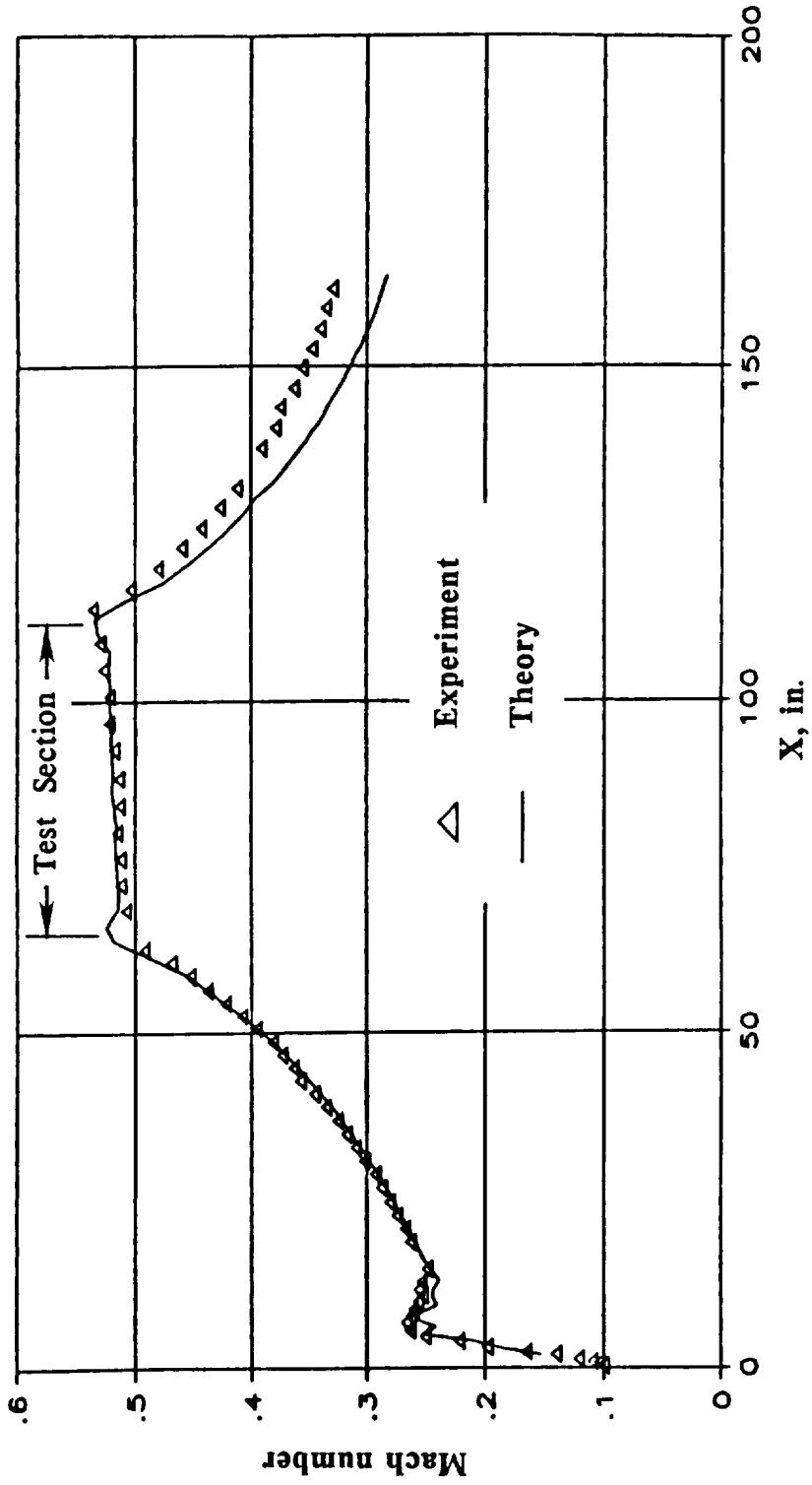

Figure 23. Predicted and experimental longitudinal Mach number distributions on tunnel wall.

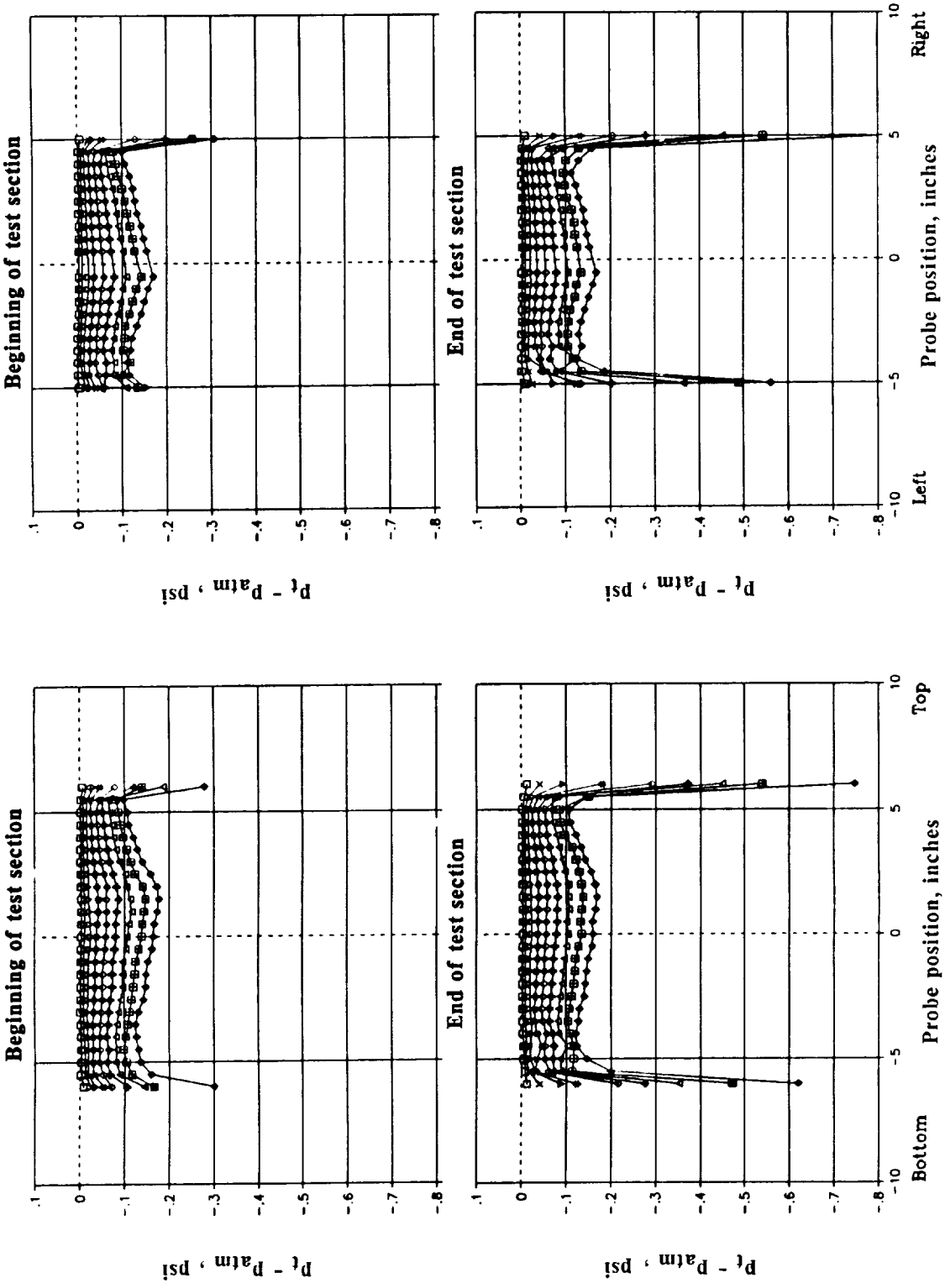

Figure 24. Original total-pressure survey of test section. Symbols represent 500-rpm increments from 500 to 4500 rpm.

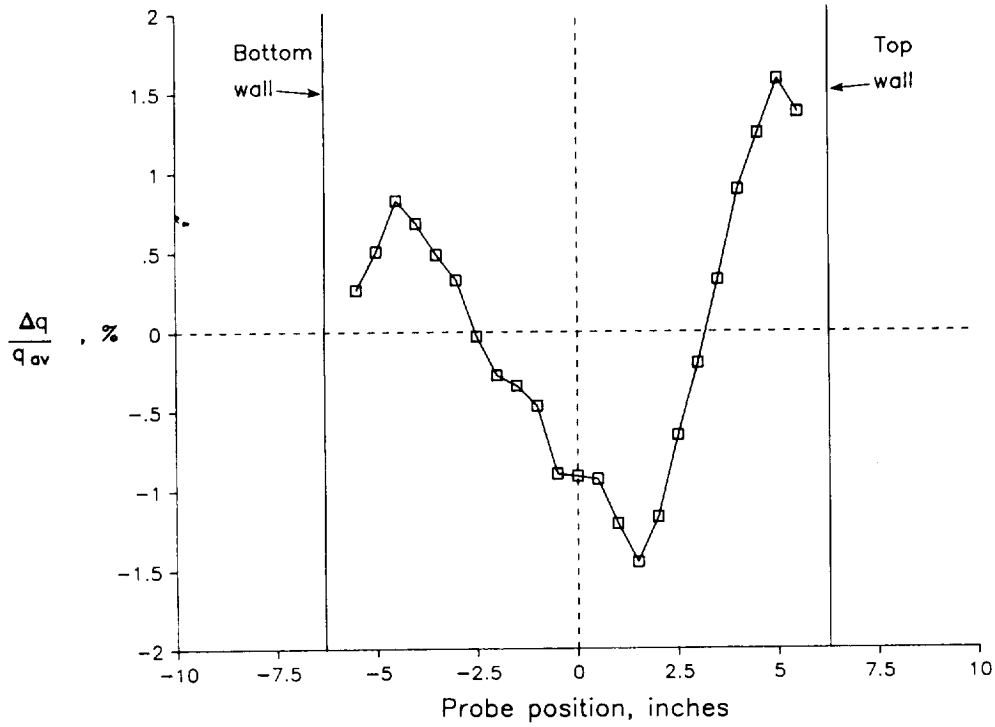

(a) Vertical survey.

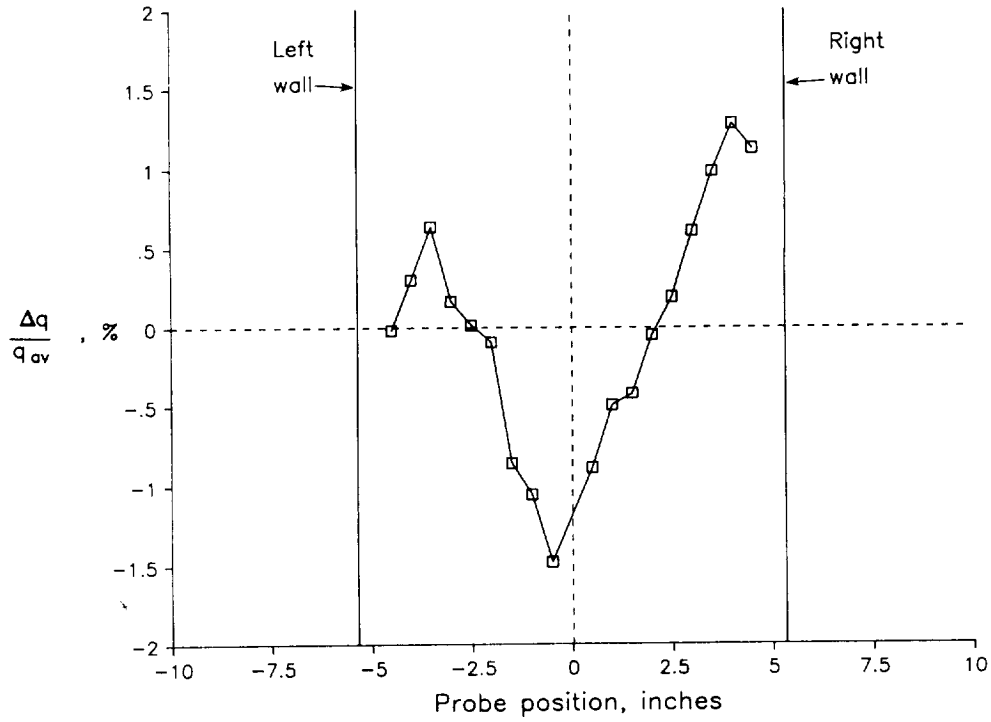

(b) Horizontal survey.

Figure 25. Dynamic pressure survey for original configuration. $M \approx 0.49$.

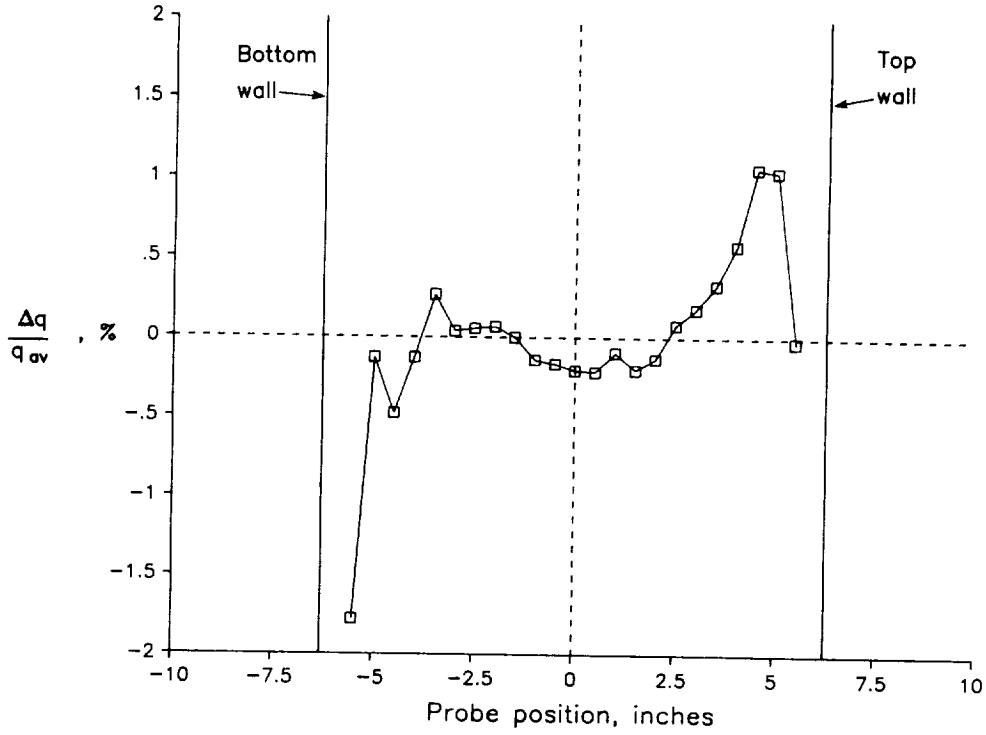

(a) Vertical survey.

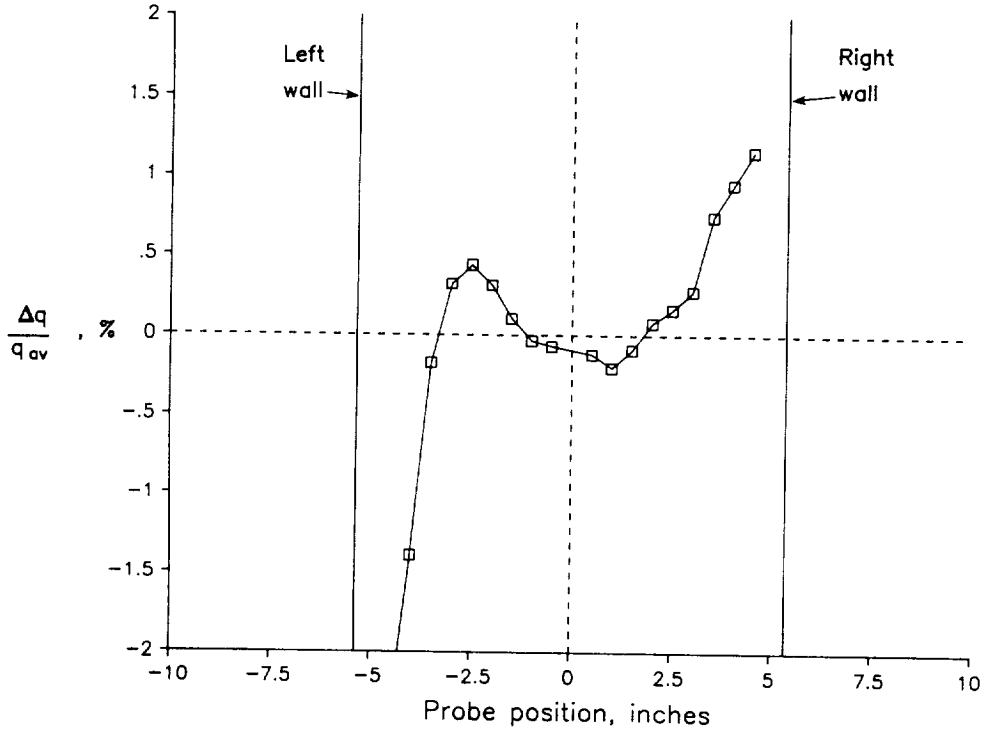

(b) Horizontal survey.

Figure 26. Dynamic pressure survey without camera pod and strut but with 1/4-in-diameter pitot probe. $M \approx 0.52$.

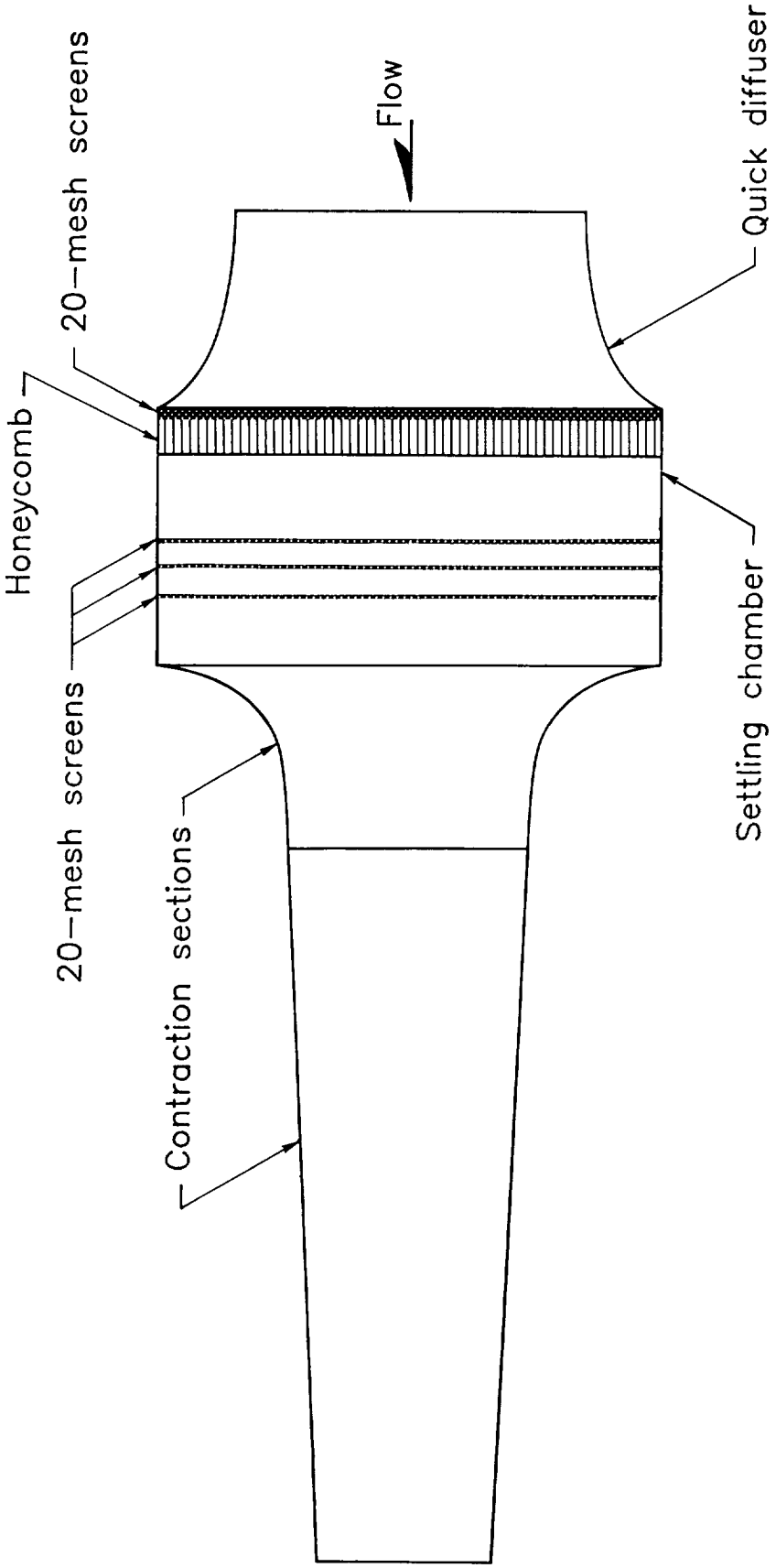

Figure 27. Quick diffuser, settling chamber, and contraction sections after addition of pressure drop screens.

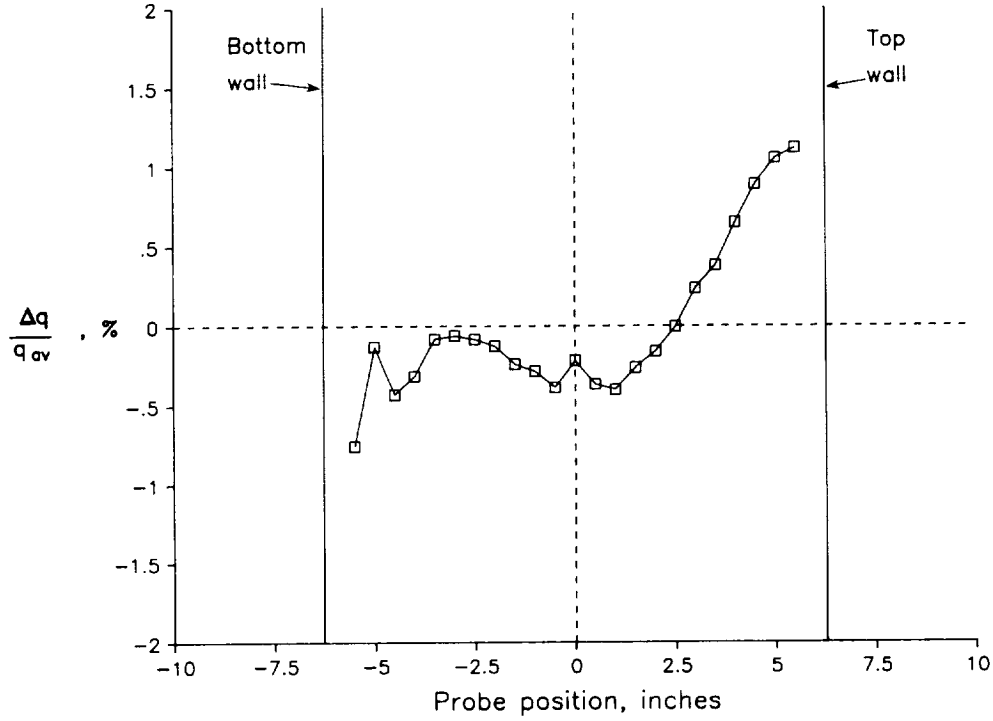

(a) Vertical survey.

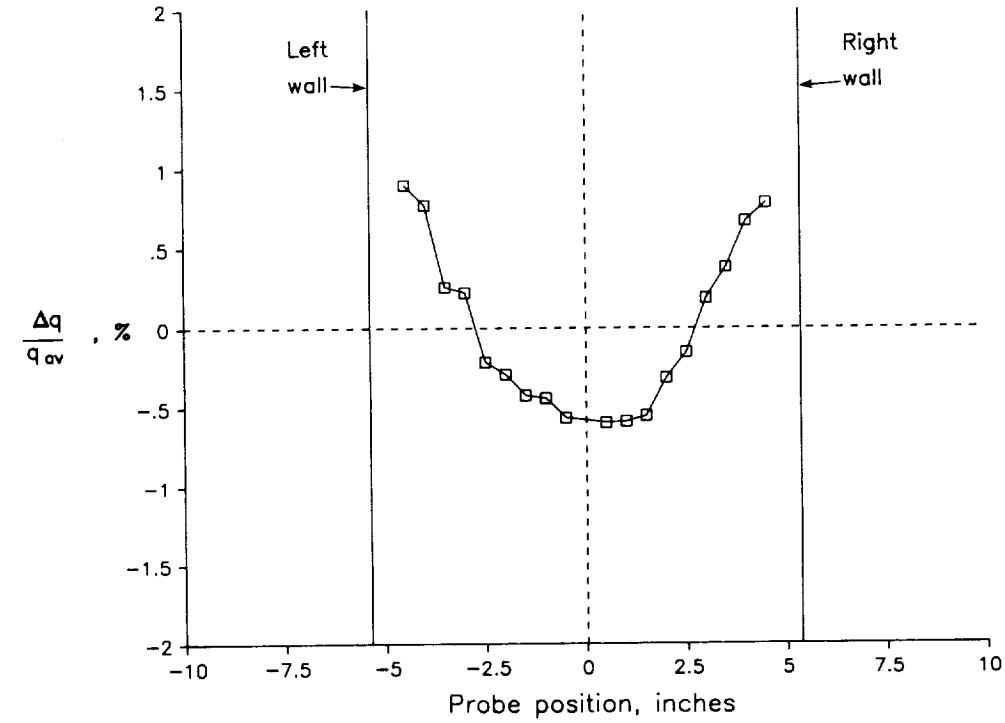

(b) Horizontal survey.

Figure 28. Dynamic pressure survey with three additional screens upstream of honeycomb. $M \approx 0.51$.

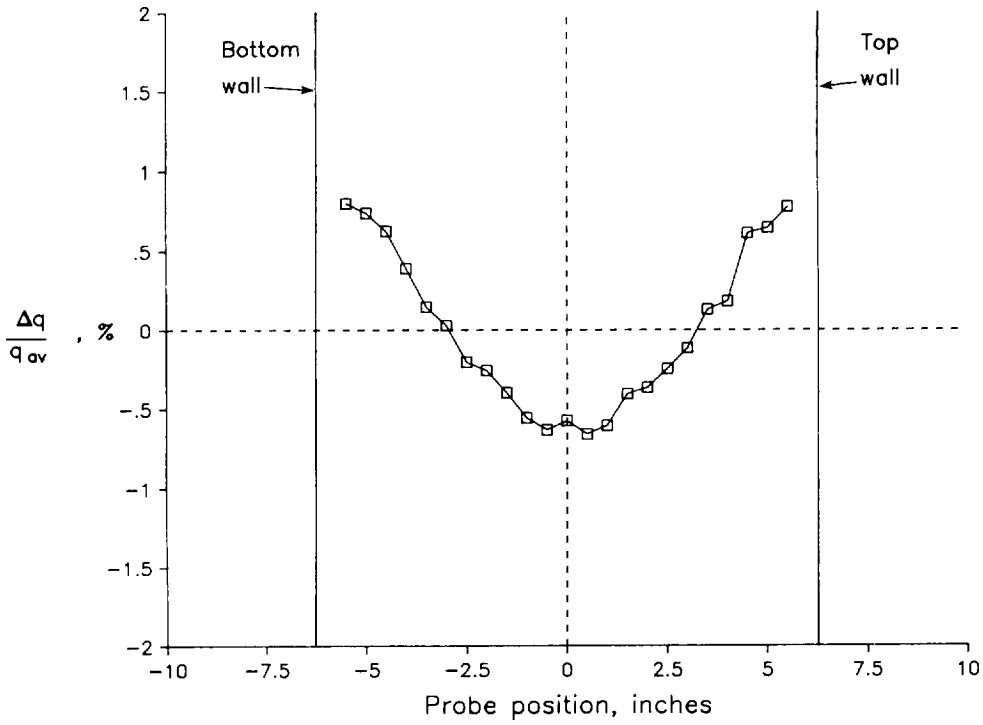

(a) Vertical survey.

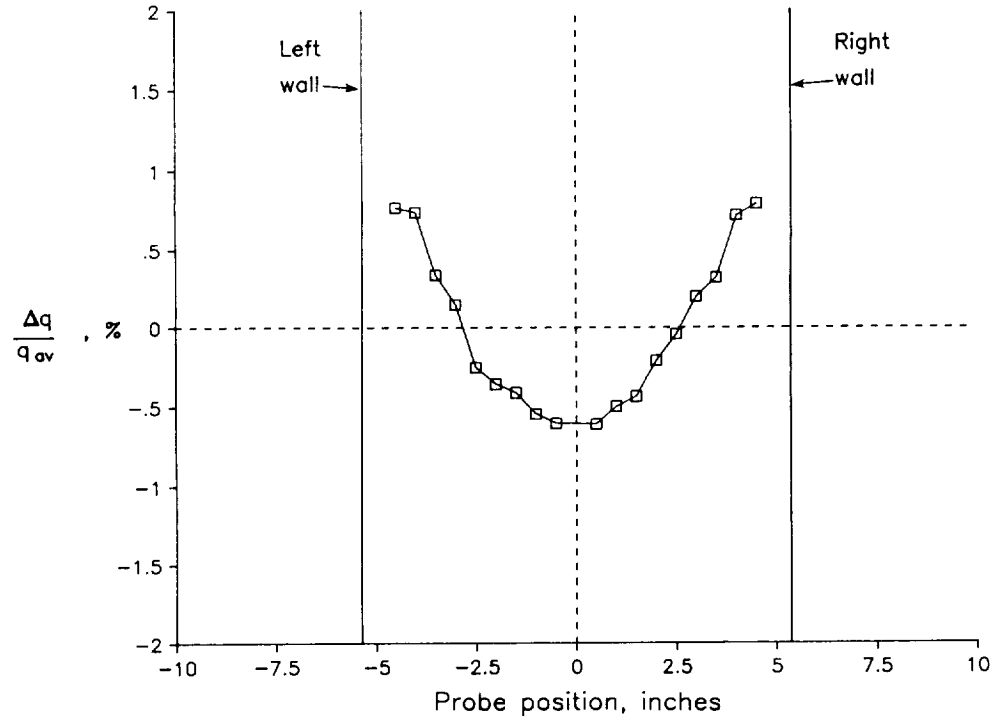

(b) Horizontal survey.

Figure 29. Dynamic pressure survey (same as fig. 28 except with 1/4-in-diameter pitot probe pulled down to tunnel wall). $M \approx 0.51$.

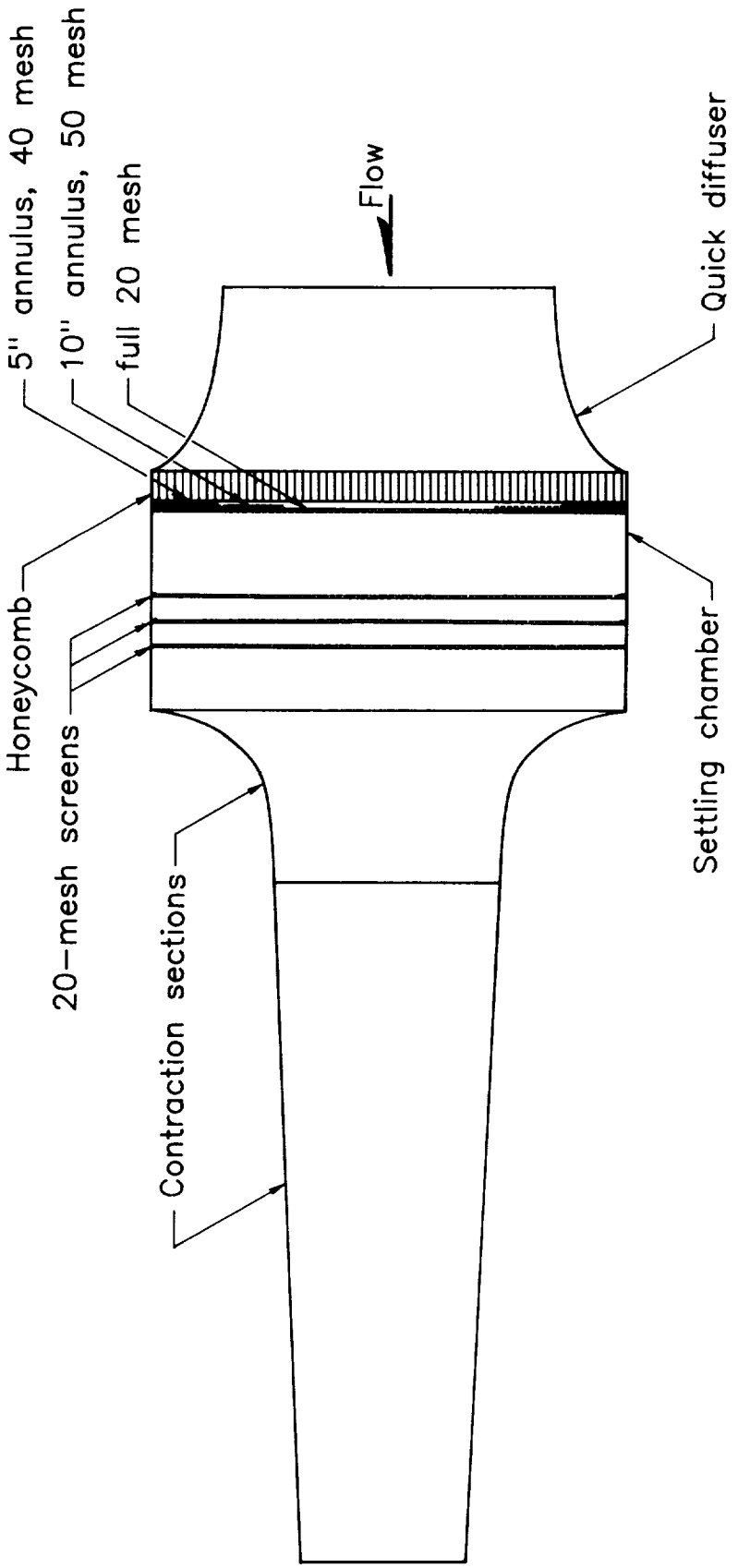

Figure 30. Quick diffuser, settling chamber, and contraction sections after various modifications.

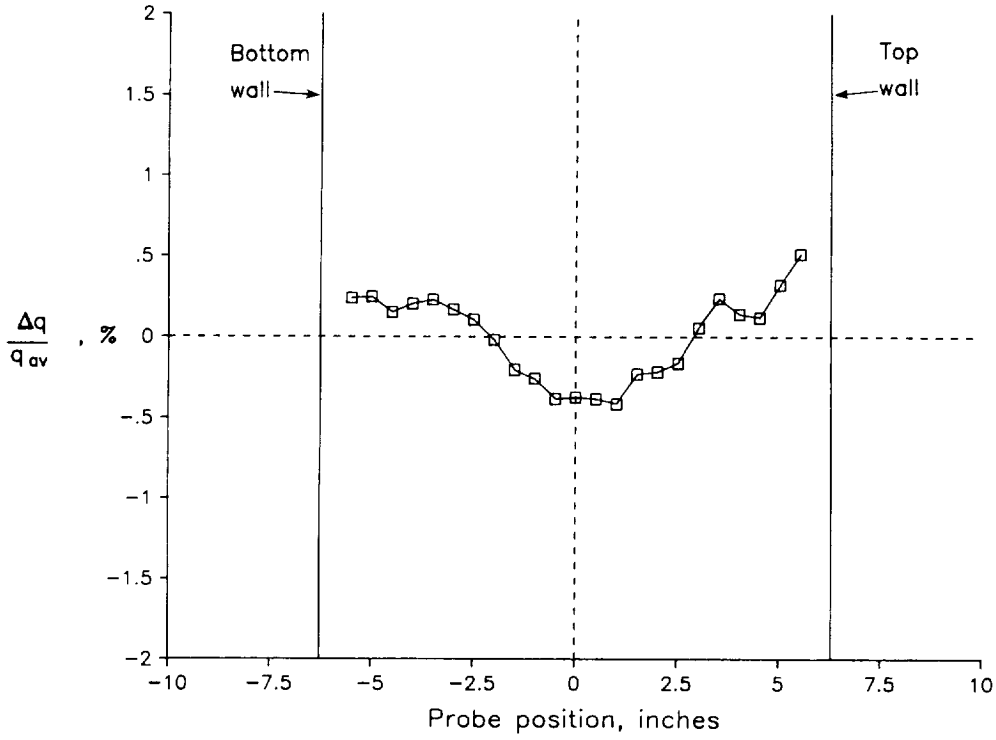

(a) Vertical survey.

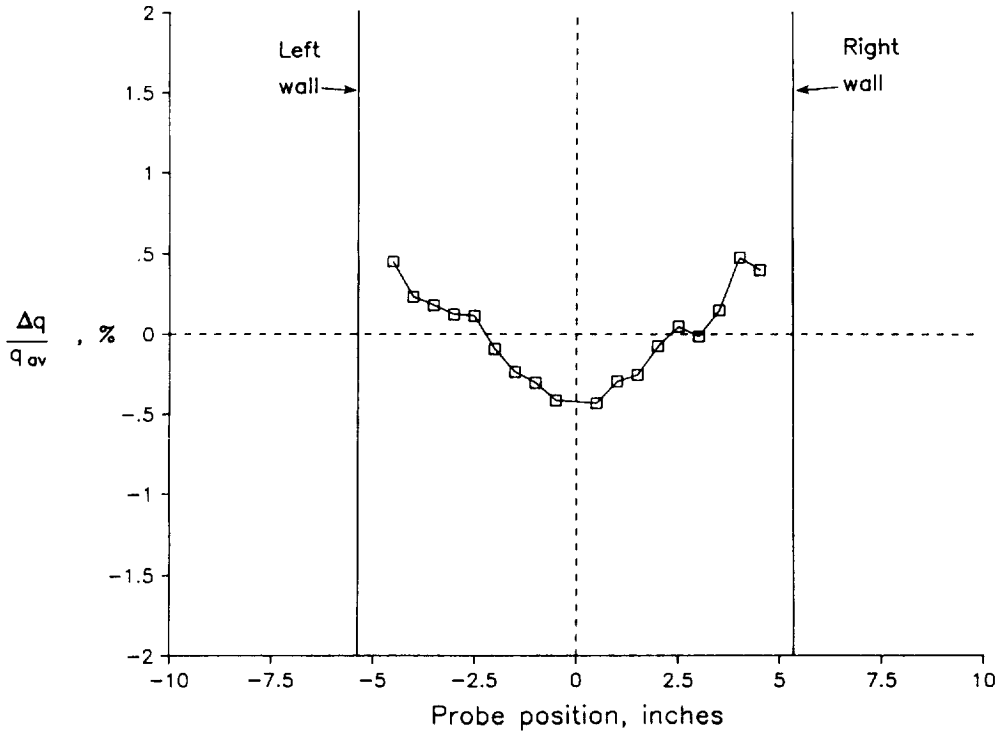

(b) Horizontal survey.

Figure 31. Dynamic pressure survey using screen-honeycomb arrangement shown in figure 30. $M \approx 0.51$.

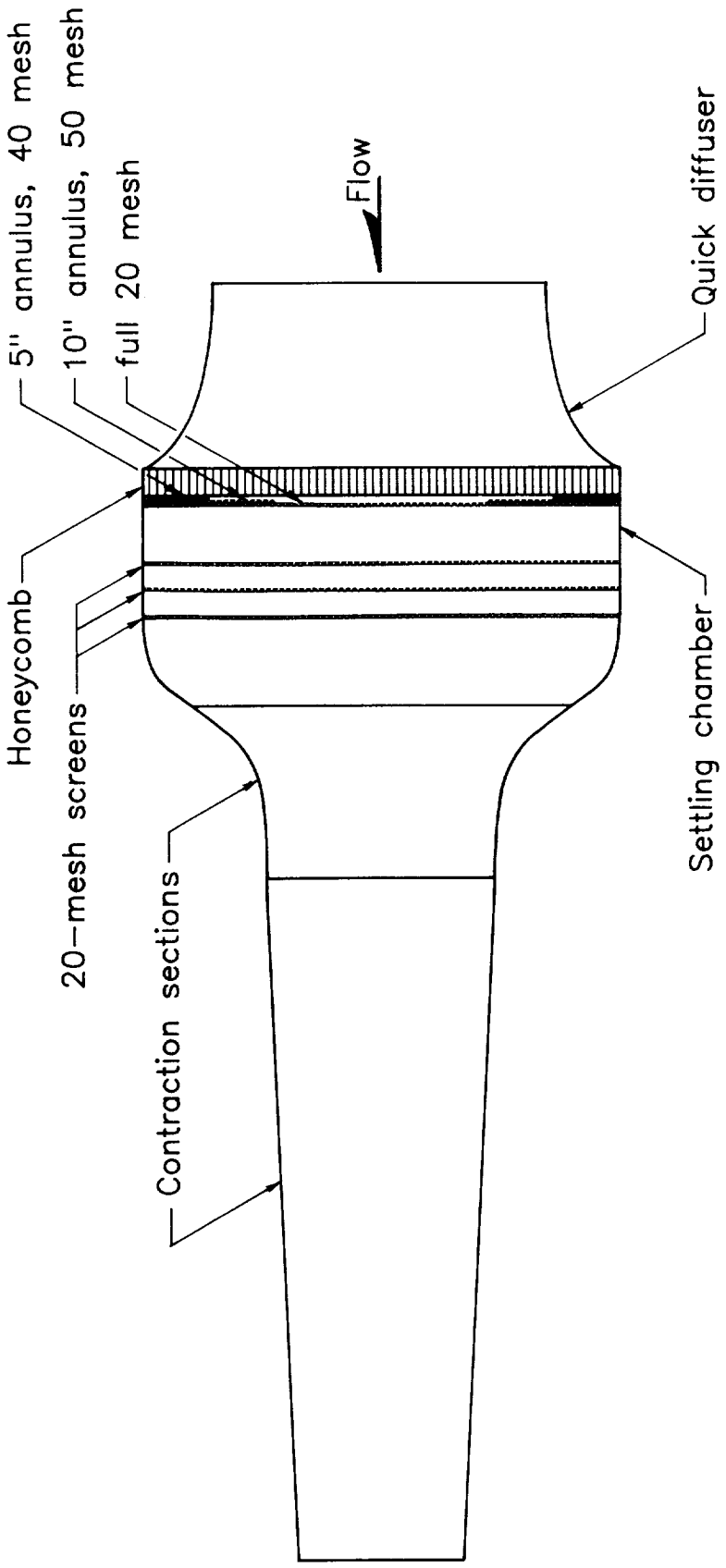

Figure 32. Present configuration of quick diffuser, settling chamber, and contraction sections.

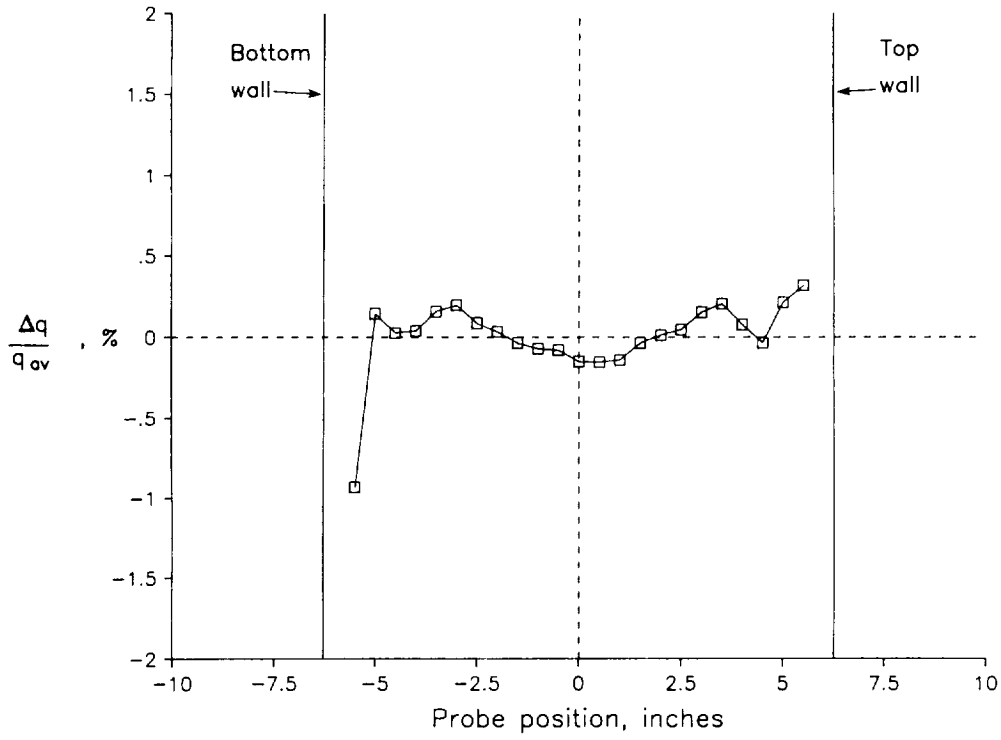

(a) Vertical survey.

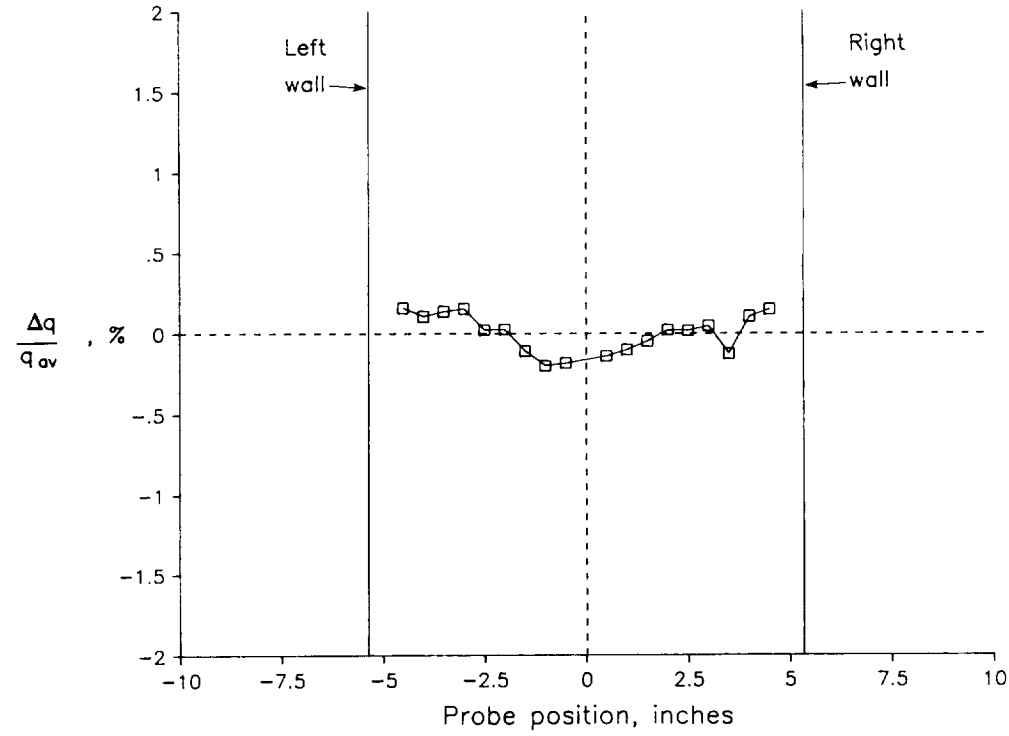

(b) Horizontal survey.

Figure 33. Dynamic pressure survey using modified primary contraction section. $M \approx 0.51$.

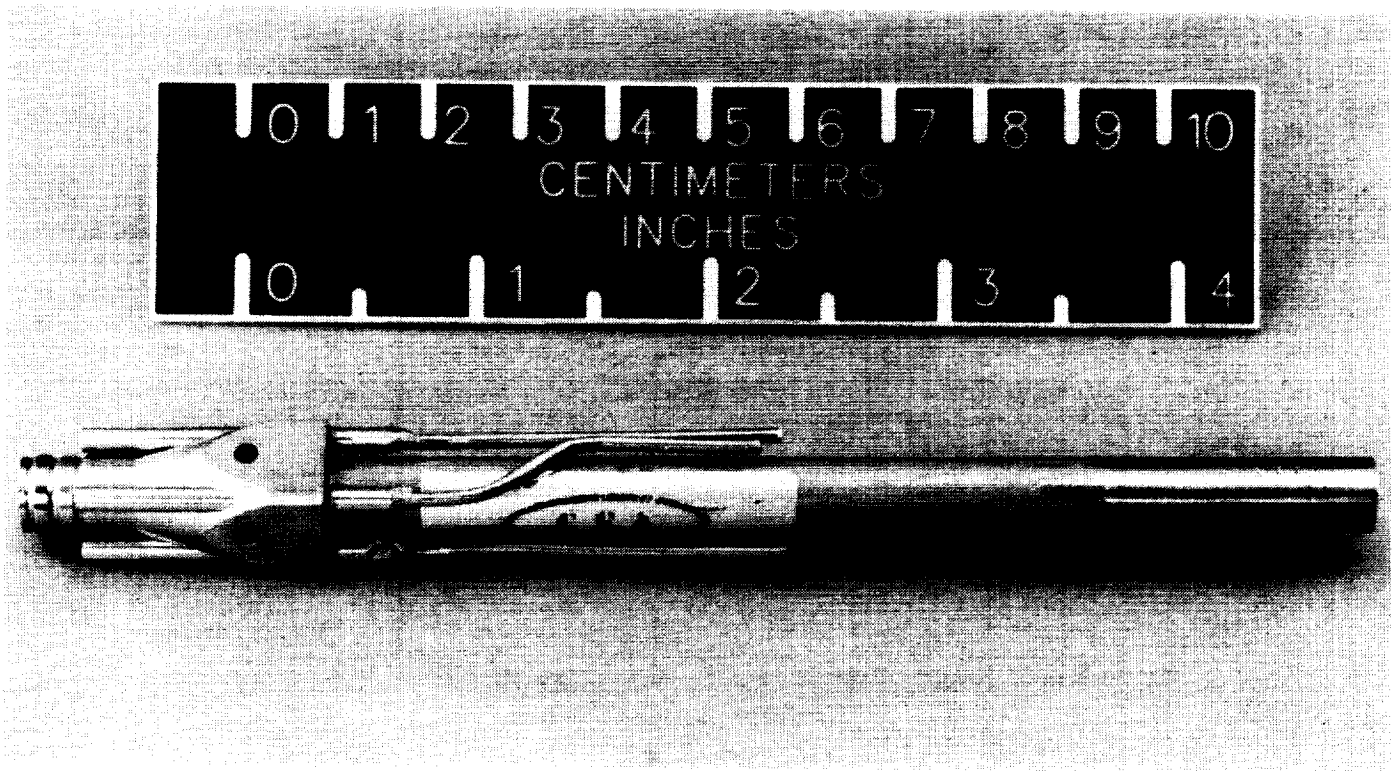

L-88-8373

(a) Side view.

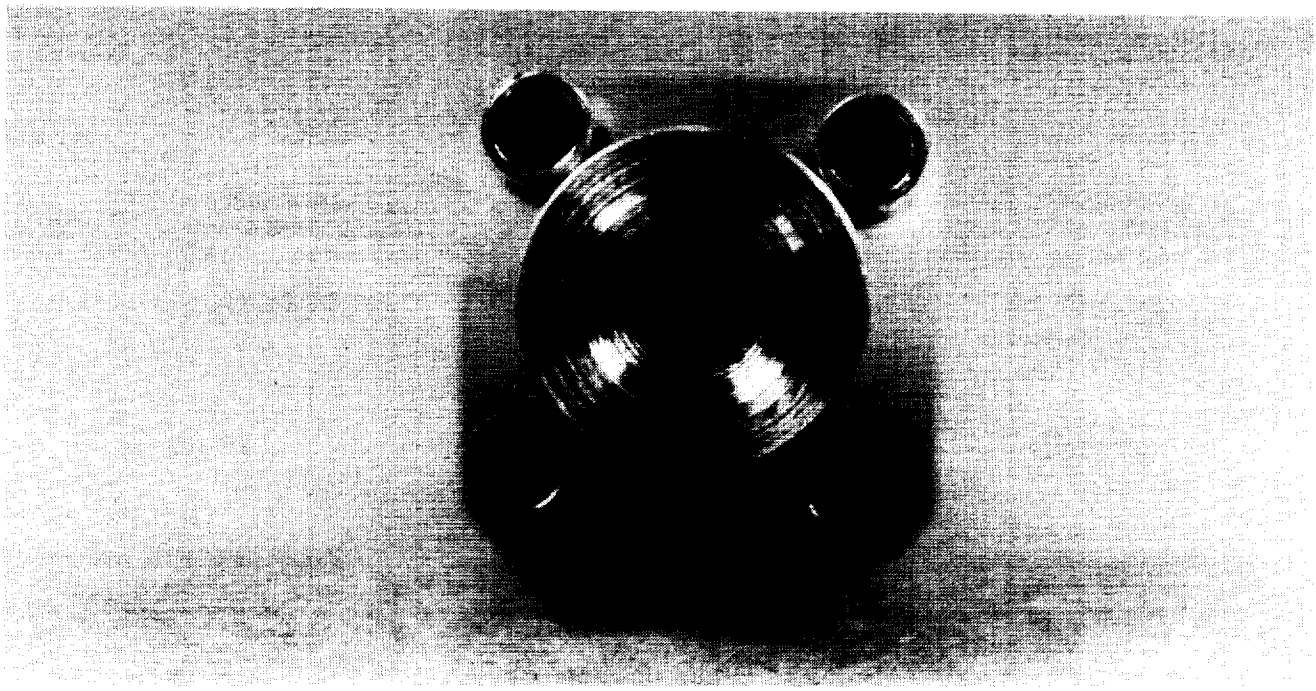

L-88-8374

(b) Front view.

Figure 34. Two-axis yawmeter.

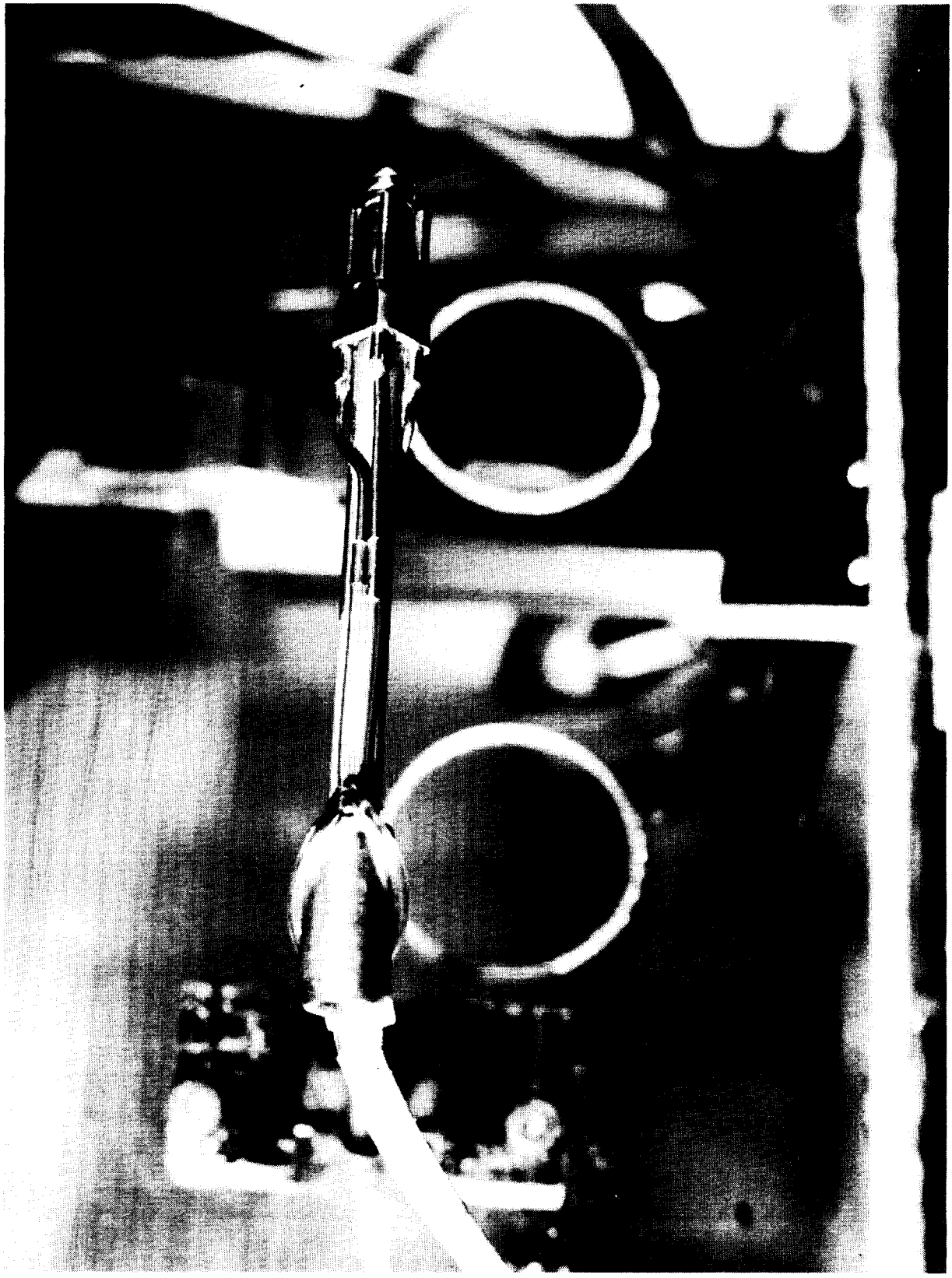

L-87-08066

Figure 35. Probe mounted in test section of 13-inch MSBS wind tunnel.

L-88-209

Figure 36. Optical cathetometer installation.

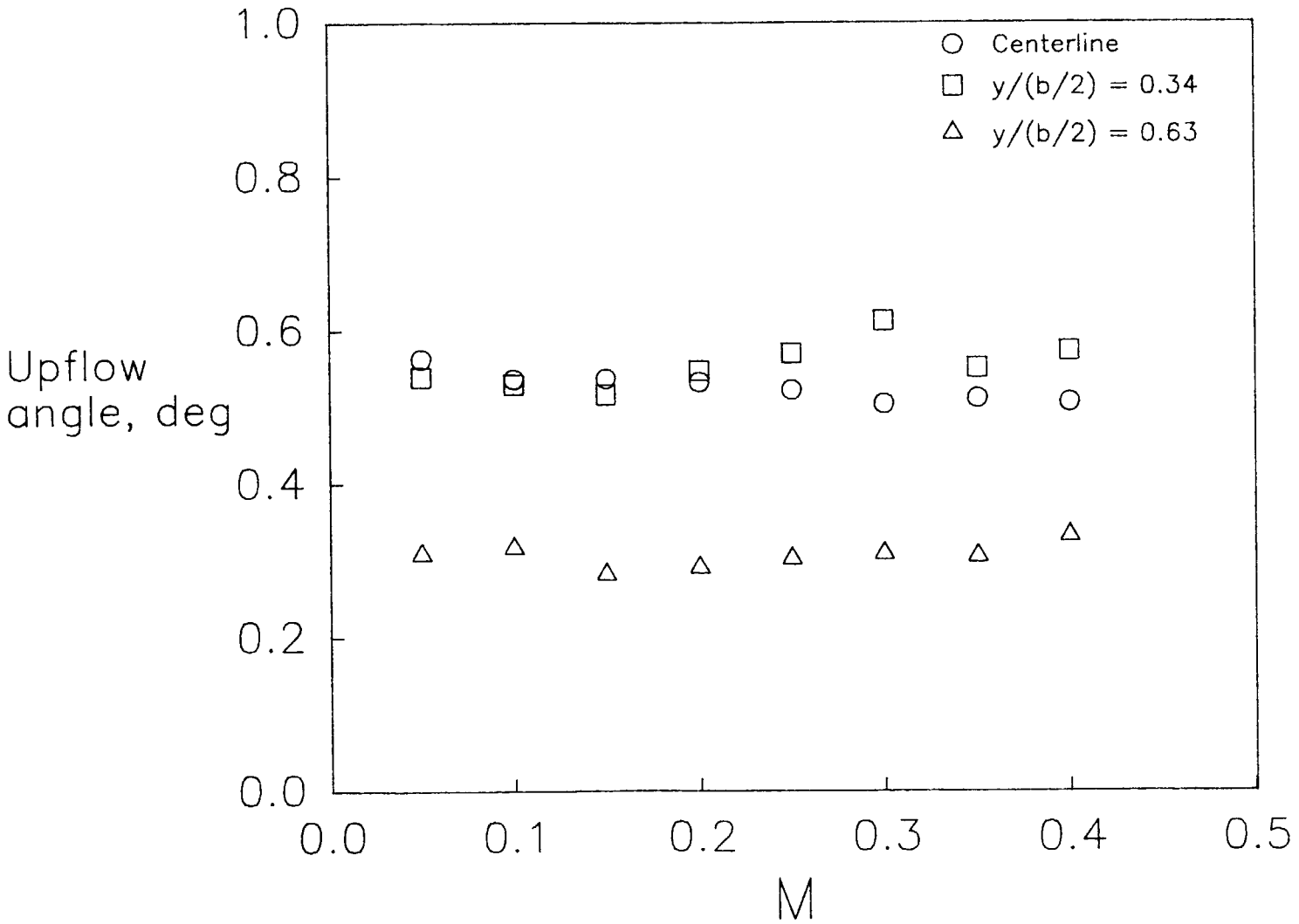

Figure 37. Upflow values of flow angularity at three spanwise locations.

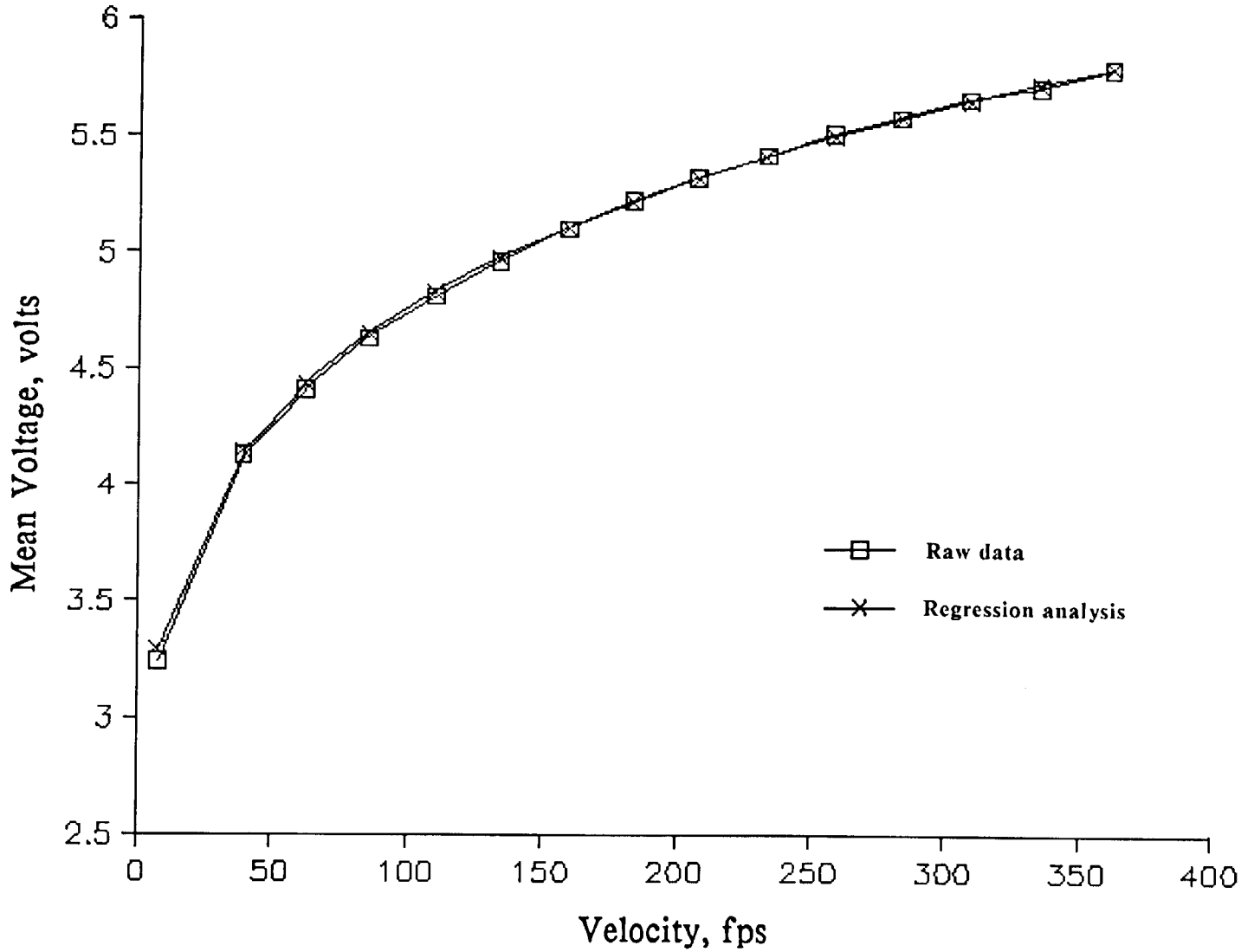

Figure 38. Typical regression analysis curve fit of velocity fluctuation calibration data.

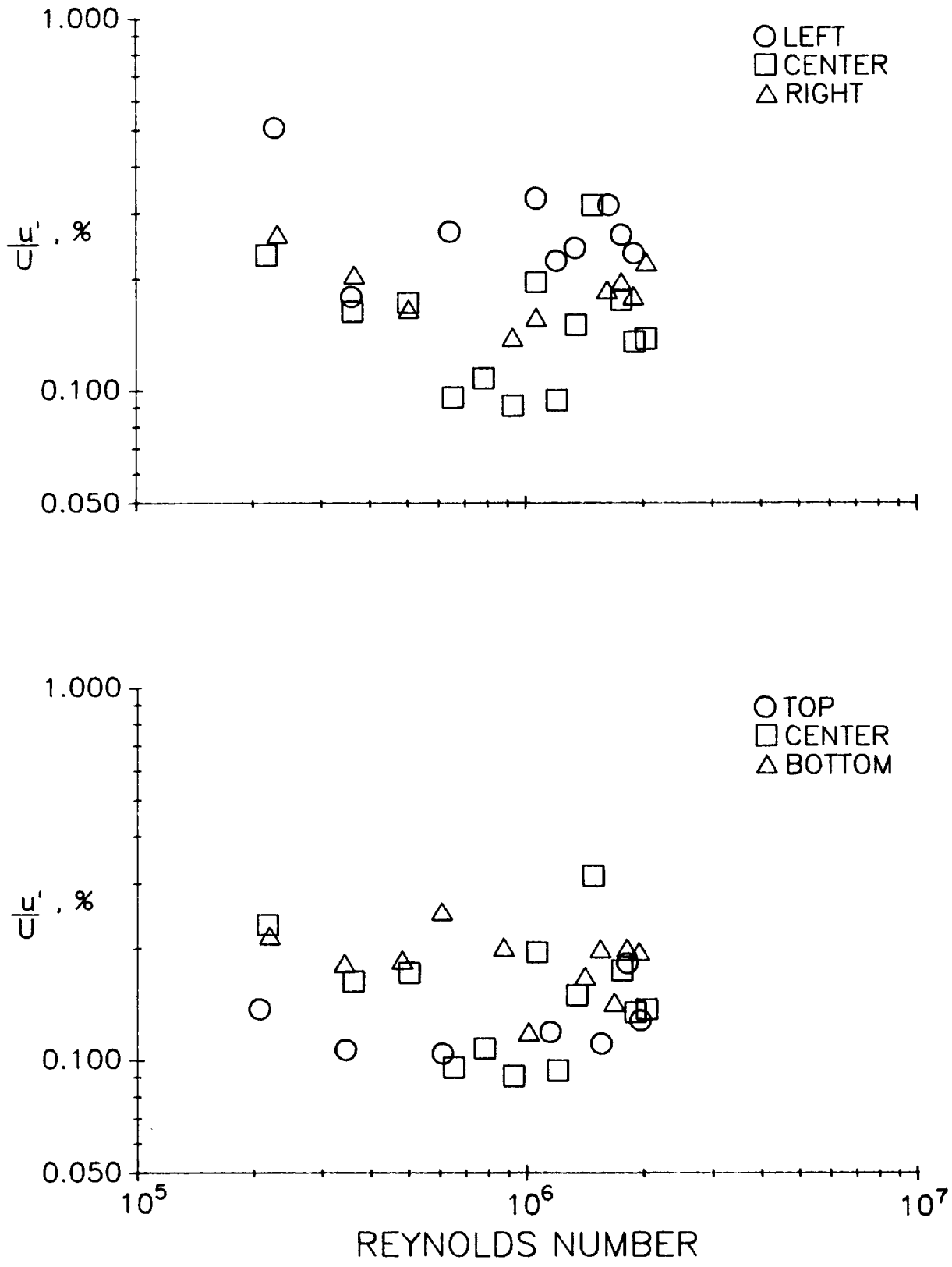

Figure 39. Horizontal and vertical scans of fluctuating velocity component u'.

NASA
National Aeronautics and Space Administration

Report Documentation Page

1. Report No.	2. Government Accession No.	3. Recipient's Catalog No.
NASA TM-4090		

4. Title and Subtitle	5. Report Date
The 13-Inch Magnetic Suspension and Balance System Wind Tunnel	January 1989
	6. Performing Organization Code
7. Author(s)	8. Performing Organization Report No.
William G. Johnson, Jr., and David A. Dress	L-16515
9. Performing Organization Name and Address	10. Work Unit No.
NASA Langley Research Center Hampton, VA 23665-5225	505-61-01-02
	11. Contract or Grant No.
12. Sponsoring Agency Name and Address	13. Type of Report and Period Covered
National Aeronautics and Space Administration Washington, DC 20546-0001	Technical Memorandum
	14. Sponsoring Agency Code

15. Supplementary Notes

16. Abstract

The Langley Research Center has a small, subsonic wind tunnel in use with the 13-inch Magnetic Suspension and Balance System (MSBS). The tunnel is capable of speeds up to Mach 0.5. This report presents tunnel design and construction details. It includes flow uniformity, angularity, and velocity fluctuation data. It also compares experimental Mach number distribution data with computed results from the General Electric Streamtube Curvature Program.

17. Key Words (Suggested by Authors(s))	18. Distribution Statement
Flow uniformity Wind-tunnel design Magnetic suspension and balance system	Unclassified—Unlimited Subject Category 09

19. Security Classif.(of this report)	20. Security Classif.(of this page)	21. No. of Pages	22. Price
Unclassified	Unclassified	46	A03

For sale by the National Technical Information Service, Springfield, Virginia 22161-2171

National Aeronautics and
Space Administration
Code NTT-4

Washington, D.C.
20546-0001

BULK RATE
POSTAGE & FEES PAID
NASA
Permit No. G-27